Energy 283 (2023) 128998

Contents lists available at ScienceDirect

Energy

journal homepage: www.elsevier.com/locate/energy

Triple-objective MPSO of zeotropic-fluid solar ejector cycle integrated with cold storage tank based on techno-economic criteria

Seyedeh Mohadeseh Miri, Mahmood Farzaneh-Gord *, Ali Kianifar

Mechanical Engineering Department, Faculty of Engineering, Ferdowsi University of Mashhad, Mashhad, Iran

ARTICLE INFO

Handling Editor: X Zhao

Keywords:
Parabolic through collector
Ejector cycle
Zeotropic fluid
Exergo-economic-environmental assessment
Triple-objective MPSO optimization

ABSTRACT

The current study objective is to optimize the integration of a solar ejector cycle with cold storage by applying a multi-objective modified particle swarm optimization technique. Various collector and working fluid's effects are evaluated on dynamic system behavior, which zeotropic fluid and parabolic trough collector have been the most effective choices. Hot and cold storage tanks are applied to overcome the instability of solar energy and ensure sustainable access to produced cold. Design parameter's optimum values are estimated through sensitivity analysis and genetic algorithm optimization which are decreased up to 70% compared to initial guesses. An artificial neural network is employed to train exergo-economic-environmental data which fed into the multi-objective modified particle swarm optimization algorithm. With using of cold storage tank, the system's coefficient of performance is enhanced up to three times compared to the ejector cycle at optimum design variable. By employing of parabolic trough collector, the system has its maximum coefficient of performance and exergy efficiency, as well as the minimum size of the ejector cycle and cold storage tank. The parabolic trough collector, air handling unit, and cold storage tank waste over 80% of the overall system's exergy. The payback period of system is estimated about 3.5 years.

1. Introduction

Using electricity from the grid to generate cold poses two primary issues: firstly, it contributes to the escalating consumption of fossil fuels, which are becoming increasingly scarce; and secondly, it results in the release of environmental pollutants, leading to significant problems [1]. One option to reduce electricity consumption is to replace high electricity-consuming systems with more efficient heat input processes like EJCs. They have several advantages, including advanced technology, simple structure, lower equipment costs, and minimal maintenance requirements [2]. A possible solution to supply heat is to utilize renewable energies, with solar energy being a particularly accessible option. However, SEJCs have challenges due to their face on variable conditions like solar radiation and ambient temperature [3]. Dynamic modeling of EJC was suggested to face these negative aspects [4]. By applying a variable area ratio for the ejector, the system's COP can be improved by up to 24% through dynamic analysis [5]. Previous studies have shown that the exergy efficiency and COP of SEJs vary throughout the day and across different months. For example, the COP was lowest during the first and last hours of the day but increased to approximately 0.7 during the middle of the day [6]. The highest and lowest COP values for SEJs were reported in July and May over a period of five months [7]. The maximum off-design COP was reported as 0.197 in August for an SEJ driven by a collector without HST over a six-month period [8]. The study by Pollerberg et al. [9] focused on a solar-driven multi-stage SEJS system with two evaporators. They found that the solar COP ranged from 0.11 to 0.29, with an average daily efficiency of 0.27. The SEJS had a COP between 0.43 and 0.53, with a maximum entrainment ratio of 0.68. Compared to the vapor compression cycle, this system has the potential to save up to 80% of electricity [10].

Due to manage cold produced from the available solar radiation intensity and required CD, energy storage technology was applied in solar-driven ERS [11]. HST helped to achieve an acceptable average temperature in the SEJS [12–15] or absorption cycles [16,17]. Moreover, an auxiliary heater further reduced its size [12]. Also, CST was identified as a potential solution for the SEJS system [2]. Allouche et al. [18] evaluated the influence of CST's capacity on SEJS's overall COP. The variation of CST's volume from 250 to 2500 L increased COP from 0.094 to 0.195, approximately. The SEJS's performance was evaluated by Diaconu et al. [19] under two with and without CST states. As the results, the system with CST achieved higher annual energy removal compared to

* Corresponding author.
E-mail addresses: mhdsh.miri@gmail.com (S.M. Miri), m.farzanehgord@um.ac.ir (M. Farzaneh-Gord), a-kiani@um.ac.ir (A. Kianifar).

https://doi.org/10.1016/j.energy.2023.128998
Received 8 June 2023; Received in revised form 26 July 2023; Accepted 2 September 2023
Available online 9 September 2023

Nomenclature

A	Area [m^2]
C	Capacity Factor – Cost [$ /h]
c	Average cost per unit of exergy [$ /Wh]
E	System rate of energy [J /s]
$\dot{E}x$	Rate of exergy [J /s]
g	Gravitation [m /s^2]
G_T	Solar intensity [Wh /m^2]
h	Enthalpy [J /kg]
i	Interest ratio
$\dot{m}$	Mass flow rate [kg /s]
n	System lifetime [year]
NN	System lifetime in a year [h]
P	Pressure [Pa]
$\dot{Q}$	heat [J /s]
r	Inflation rate [%]
R	CST thermal resistance [(m^2K) /W]
s	Entropy [J /(kg K)]
t	Time [s]
T	Temperature [°C]
U	Overall heat transfer coefficient [W /m^2.K]
v	Velocity [m /s]
V	Storage Tank capacity [m^3]
$\dot{W}$	work [J /s]
z	Elevation [m]- Capital cost [$]

Abbreviation

AHU	Air Handling Unit
ANN	Artificial Neural Network
ave	average
CD	Cooling Demand
COP	Coefficient of Performance
CST	Cold Storage Tank
DPR	Detailed Payback period Ratio
Eff	Effectiveness
EJC	EJector Cycle
ETC	Evacuated Tube Collector
Exd	Exergy destruction
FPC	Flat Plate Collector
GA	Genetic Algorithm
GWP	Global Warming Potential
HST	Hot Storage Tank
Inv	Inverse
MPSO	Modified Particle Swarm Optimization
ODP	Ozone Depletion Potential
PSUC	Product Sum Unit Cost
PTC	Parabolic Through Collector
SEJS	Solar EJector System
SEJHCST	Solar-powered Ejector cycle integrated with Hot and Cold Storage Tanks
WF	Working Fluid
Ex.Va	Expansion Valve

Subscript

Am	Ambient
ch	charge
Co	Condenser
coll	Collector
dc	discharge
envr	environment
Ev	Evaporator
Ge	Generator
h	hour
Inv	investment
l	liquid
le	Leakage
O.M	Operation and maintenance
Pu	Pump
s	Supply circuit/solid
sol	Solar
th	thermal
us	Useful

Greek letter

η	Efficiency
μ	Entrainment ratio
ξ	pollutant emission [kg /kWh]
ρ	Density [kg /m^3]

another. Dennis et al. [20] investigated a variable geometry ejector integrated with CST, which could increase yield by 8–13% compared to fixed geometry one. Worall et al. [21] and Eames et al. [22] studied experimentally the SEJS integrated with CST. Also, more stable COP were reported by using CST with SEJS [23]. Different types of collectors were also compared in terms of cost-effectiveness and efficiency. FPC, double-glazed FPC, and ETC collectors were evaluated by some researchers. Pridasawas and Lundqvist [15] found that while FPC had the lowest cost, it required an auxiliary heater and was not considered economically viable. ETC had higher efficiency but was not cost-effective [24]. In terms of exergy efficiency [25] and also to achieved a higher solar fraction [26], ETC performed the best, followed by double- and single-glazed FPCs. Vidal et al. [18] reported a maximum hourly COP of 0.39 for an SEJS powered by FPC, while Varga et al. [12] achieved a COP of less than 0.6 using ETC. In an office building air conditioning application in Shanghai, an ETC area equal to 15 m^2 could provide an average hourly COP of up to 0.48 [10].

In order to make the ejector system more economically attractive, some studies have been optimized the ejector geometry and its effects on system performance or changed the ejector cycle's configuration. Regarding the ejector geometry optimization, the various parameters related to ejector geometry such as area ratio [27–33], Nozzle exit position (NXP) [34–42] were optimized in previous works. Regarding the ejector performance improvement, reducing the mechanical pump work in ejector cycles has been considered by using gravitational ejector [43], bi-ejector system [44,45] and thermal pumping effect [46,47]. Regarding the changing the ejector cycle's configuration, applying the multi-component systems have been assessed such as additional jet pump [48,49], multi-stage ejector [50,51] or multi-evaporator ejector cycle [52,53] etc. Not only two mentioned approaches above were not considered, but also determining the optimum operation condition of system was made to interest in present study. Not only two mentioned approaches above were not intended, but also the optimization main approach in present study is to find the optimum operation condition of system which some previous researches [15,18] have been addressed to it.

- **The novelty and research motivation**

Dynamic modeling of SEJHCST was focused on evaluating ETC and FPC performance with pure refrigerants [15,18]. Thermo-economic-environmental modeling of PTC and its effects on SEJHCST performance has not been found in previous literature. WF's characteristics should be in accordance with high temperatures

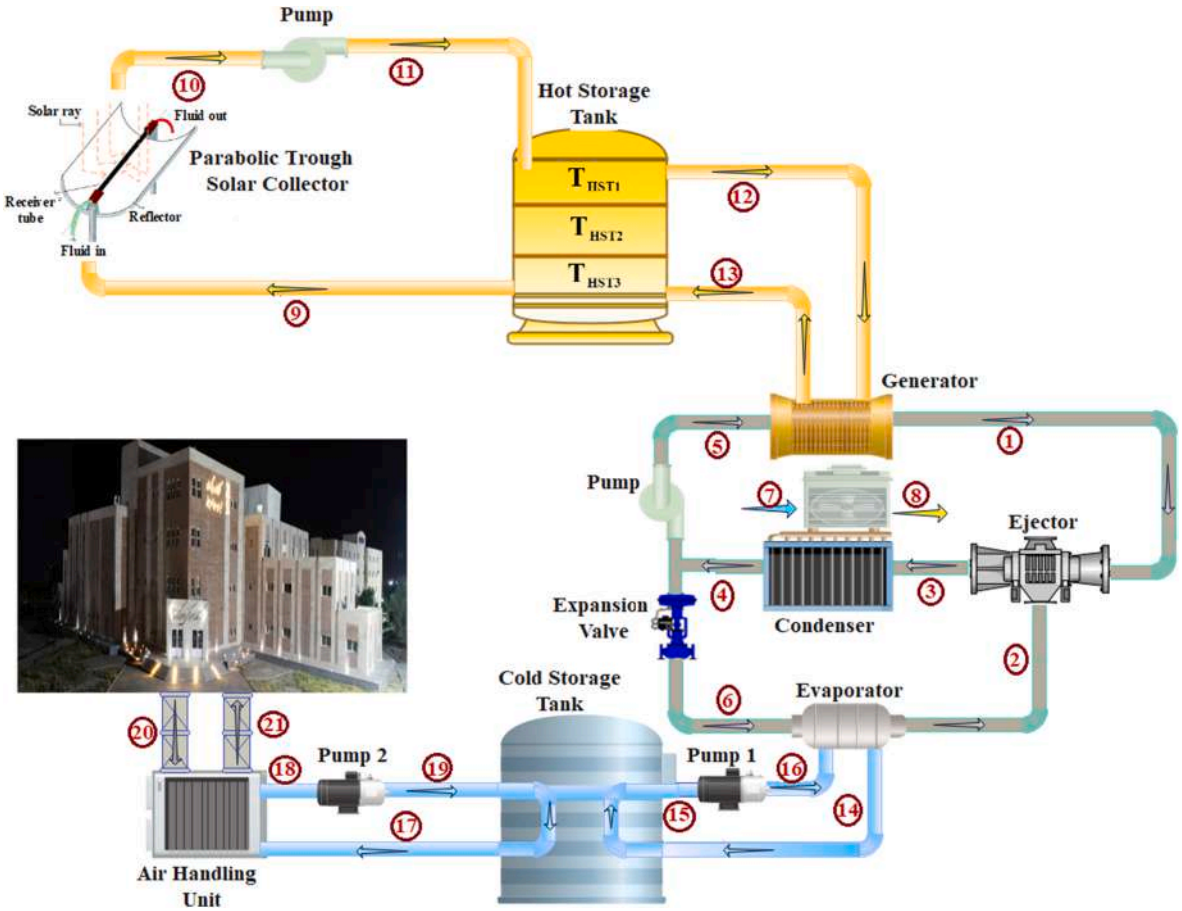

Fig. 1. Schematic diagram of the investigated SEJHCST.

accessible by PTC. New generation refrigerants, namely zeotropic fluids, have temperature glide characteristics which can cover variable intensity of solar radiation and phase change process. While some previous research has investigated the zeotropic fluid influence alone EJC performance [54–56], this study focuses on SEJHCST performance using zeotropic fluid.

As reviewed previous literatures, the Ref.s number [15,18] have been optimized their investigated system based on thermodynamic criteria. Thermo-economic-environmental aspects have not been seen in previous literature by author for ejector cycle optimization especially by using of advanced optimization techniques like triple-objective MPSO optimization. In present study, a two-stage optimization approach is used to find the optimum operation condition, system sizing, and performance based on exergo-economic-environmental criteria. Firstly, a one-objective GA beside sensitivity analysis is applied to determine the optimum design variable, followed by ANN integrated to triple-objective MPSO to identify the optimum system size and performance.

2. System description

The ejector device can be used in low thermal energy cycles such as solar-powered or feed-waste-heat systems. Two input flows with different properties enter, mixe, and then exit with new properties. Input heat from the generator plays a stimulus role to suck secondary flow from the evaporator [57]. In this study, a SEJS integrated with HST is considered to operate during sunny hours from 5 a.m. to 6 p.m. Also, a CST is used to manage supply and demand of refrigeration, which connects two feed circuits into the refrigeration cycle and consumption place (Fig. 1).

The following assumptions are considered here:

- Pressure-constant and mixing regime are assumed for ejector modeling [58].
- The open-type HST is considered with stratified temperature along height coordinate and constant temperature value at each of the layer [59].
- The closed-type CST is considered which was estimated more stable with high cold replacement rate based on Bi et al.'s results [60].
- Two charge and discharge processes are considered, which were accurate enough to investigate CST performance [61].
- Potential and kinetic energy rates are neglected for all equipment except for the ejector [58].
- Friction and mixing losses in nuzzle, diffuser, and mixing sections of the ejector are considered by defining the efficiency for each of them [58].

The flowchart of the modeling process is shown in Fig. 2.

3. System modeling

In this section, SEJHCST is evaluated based on three basic laws. Moreover, the system economic and environmental modeling are presented.

3.1. Mass, energy and exergy balance equations

The general mass, energy, and exergy equations can be found in general references [59]. The governing equations of various components behavior (e.g., ejector, collector, HST, and CST) are extensively expressed below.

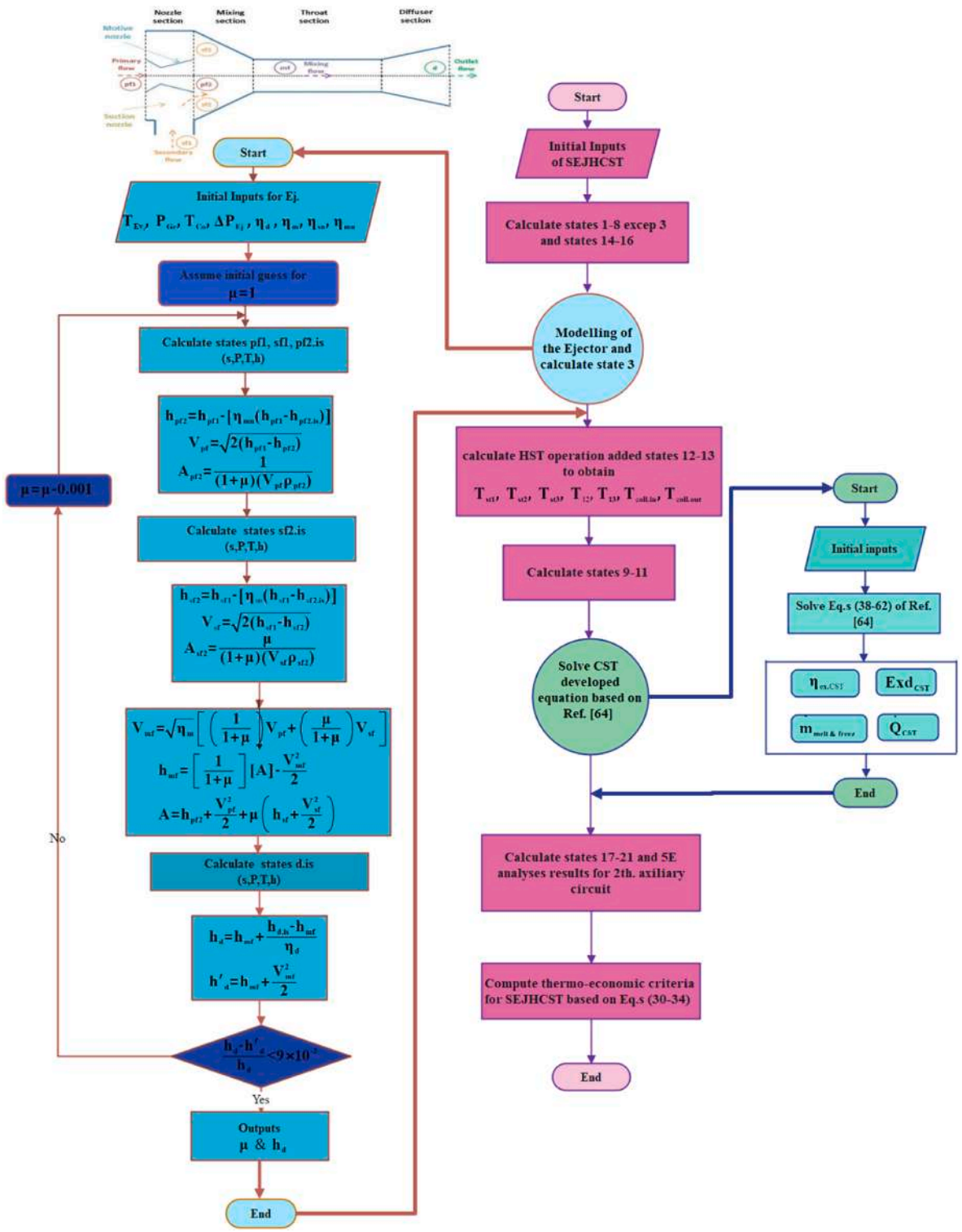

Fig. 2. The flowchart of the thermo-economic-environmental modeling for SEJHCST.

Table 1
First and second-order coefficients of the collector's efficiency [66].

Type of collector	FPC	ETC	PTC
a_{coll}	0.765	0.687	0.689
b_{coll}	0.508	1.505	0.36
c_{coll}	0.007	0.011	0.0011

3.1.1. Ejector

The ejector can replace to a compressor or expansion valve in thermodynamic cycles, improving system performance by recovering lost work from the expansion valve [5,62]. However, its one drawback is low performance [63]. The ejector performance depends on the pressure difference between two entering fluids. The primary flow enters the ejector through a convergent–divergent nozzle, accelerating the generator's coming flow from subsonic to supersonic velocity and creatting a low-pressure region at the nozzle exit. This entrains the secondary flow from the evaporator. In essence, the ejector has both a suction and pumping effects. The two streams mix together and third stream is formed with the average thermodynamic properties of two incoming streams [62]. The governing equations of ejector various parts can be achieved in the system solution-procedure flowchart shown in Fig. 2.

3.1.2. Solar collector

The total available radiation energy received by the collector aperture is obtained by Ref. [17]:

$$Q_{sol} = A_{coll} G_T \tag{1}$$

The collector's thermal efficiency is calculated by:

$$\eta_{coll} = a_{coll} - b_{coll}\left(\frac{T_{coll.in} - T_{Am}}{G_T}\right) - c_{coll}\frac{(T_{coll.in} - T_{Am})^2}{G_T} \tag{2}$$

The constant coefficients for various collectors are represented in Table 1. Solar collector efficiency is defined as its capability to transform solar irradiation into useful thermal power [65]. The received useful energy is achieved from:

$$Q_{us} = \eta_{coll} \times Q_{sol} \tag{3}$$

The thermal oil's energy balance results as follows:

$$Q_{us} = \dot{m}_{coll} C_{p.Therminol-VP1}(T_{coll.out} - T_{coll.in}) \tag{4}$$

where, $\dot{m}_{coll}$, $T_{coll.out}$ and $T_{coll.in}$ are the mass flow rate, entrance and exit flows of collector circuits, respectively.

3.1.3. Thermal storage tank

- Hot storage tank

The thermal mixing zones model is used for HST evaluation [67], at which HST should be divided into separate zones with constant temperatures. The temperature decreases from top to bottom of HST's height. The energy balance for these HST's zones can be written as follows:

Table 2
Energy and exergy balance equations for various equipment of SEJHCST.

Equipment	Energy balance	Exergy balance
Ev	$\dot{Q}_{Ev} = \dot{m}_2(h_2 - h_6)$ $\dot{Q}_{Ev} = \dot{m}_{14}(h_{14} - h_{16})$	$\dot{S}_{gen-Ev} = \begin{bmatrix}\dot{m}_2(s_2 - s_6)\\ +\dot{m}_{14}(s_{14} - s_{16})\end{bmatrix}$ $\dot{E}x_{d.Ev} = \begin{bmatrix}(\dot{E}x_2 - \dot{E}x_6)\\ +(\dot{E}x_{16} - \dot{E}x_{14})\end{bmatrix}$
Ej	$\dot{m}_2 h_2 + \dot{m}_1 h_1 = \dot{m}_3 h_3$	$\dot{S}_{gen.Ej} = \dot{m}_3 s_3 - (\dot{m}_1 s_1 + \dot{m}_2 s_2)$ $Exd_{Ej} = Ex_1 + Ex_2 - Ex_3$
Ge	$\dot{Q}_{Ge} = \dot{m}_1(h_1 - h_5)$ $\dot{Q}_{Ge} = \dot{m}_s(h_{13} - h_{12})$	$\dot{S}_{gen-Ge} = \begin{bmatrix}\dot{m}_1(s_1 - s_5)\\ +\dot{m}_s(s_{12} - s_{13})\end{bmatrix}$ $\dot{E}x_{d.Ge} = \begin{bmatrix}(\dot{E}x_5 - \dot{E}x_1)\\ +(\dot{E}x_{13} - \dot{E}x_{12})\end{bmatrix}$
Co	$\dot{Q}_{Co} = \dot{m}_3(h_4 - h_3)$ $\dot{Q}_{Co} = \dot{m}_7(h_8 - h_7)$	$\dot{S}_{gen-Co} = \begin{bmatrix}\dot{m}_3(s_4 - s_3)\\ +\dot{m}_7(s_8 - s_7)\end{bmatrix}$ $\dot{E}x_{d.Co} = \begin{bmatrix}(\dot{E}x_4 - \dot{E}x_3)\\ +(\dot{E}x_8 - \dot{E}x_7)\end{bmatrix}$
Pu of Ej	$\dot{W}_{Pu_{Ej}} = \dot{m}_1(h_5 - h_4)$ $\eta_{Pu_{Ej}} = \frac{h_{5,is} - h_4}{h_5 - h_4}$	$\dot{S}_{gen.Pu_{Ej}} = \dot{m}_1(s_5 - s_4)$ $Exd_{Pu_{Ej}} = \dot{W}_{Pu_{Ej}} + Ex_4 - Ex_5$
Ex.Va	$h_4 = h_6$	$\dot{S}_{gen.Ex.Va} = \dot{m}_3(s_6 - s_4)$ $\dot{E}xd_{Ex.Va} = \dot{E}x_4 - \dot{E}x_6$
Coll	$\dot{Q}_{us} = \dot{m}_{coll} C_{p.Therminol-VP1}(T_{10} - T_9)$	$\dot{S}_{gen.coll} = \dot{m}_{coll}(s_{10} - s_9)$ $Exd_{coll} = Ex_9 - Ex_{10}$
HST	$m_i c_p \frac{dT_i}{dt} = \begin{bmatrix}\dot{m}_{coll} c_p(T_{i-1} - T_i)\\ -\dot{m}_{12} c_p(T_{i+1} - T_i)\\ -(UA)_i(T_i - T_{Am})\end{bmatrix}$	$\dot{S}_{gen.HST} = \begin{bmatrix}\dot{m}_{coll}(s_9 - s_{10})\\ +\dot{m}_{12}(s_{12} - s_{13})\\ -\frac{\dot{Q}_{loss}}{T_{Ev}}\end{bmatrix}$ $Exd_{HST} = \begin{bmatrix}(\dot{E}x_{10} - \dot{E}x_9)\\ +(\dot{E}x_{13} - \dot{E}x_{12})\\ +\dot{Q}_{loss}\left(1 + \frac{T_0}{T_{ave}}\right)\end{bmatrix}$
CST	$\dot{Q}_{CST} = -\dot{Q}_{17-19} + \dot{Q}_{14-15} + \dot{Q}_{le}$	$\dot{S}_{gen.CST} = \begin{bmatrix}-\frac{1}{T_0}\dot{Q}_{le} - \frac{1}{T_{15}}\dot{Q}_{14-15}\\ -\frac{1}{T_{17}}\dot{Q}_{17-19} + \Delta\dot{S}_{CST.fusion}\end{bmatrix}$ $\dot{E}x_{d.CST} = T_0 \dot{S}_{gen.CST}$
Coll circuit's Pu	$\dot{W}_{Pu_{coll}} = \dot{m}_{coll}(h_{11} - h_{10})$ $\eta_{Pu_{coll}} = \frac{h_{11,is} - h_{10}}{h_{11} - h_{10}}$	$\dot{S}_{gen.Pu_{coll}} = \dot{m}_{coll}(s_{11} - s_{10})$ $Exd_{Pu_{coll}} = \dot{W}_{Pu_{coll}} + Ex_{10} - Ex_{11}$
Pu1	$\dot{W}_{Pu1} = \dot{m}_{14}(h_{16} - h_{15})$ $\eta_{Pu1} = \frac{h_{16,is} - h_{15}}{h_{16} - h_{15}}$	$Ed_{Pu1} = T_0 \times \left[\dot{m}_{14} C_{p.15} \ln\frac{T_{16}}{T_{15}}\right]$ $Exd_{Pu1} = \dot{W}_{Pu1} + Ex_{15} - Ex_{16}$
Pu2	$\dot{W}_{Pu2} = \dot{m}_{17}(h_{19} - h_{18})$ $\eta_{Pu2} = \frac{h_{19,is} - h_{18}}{h_{19} - h_{18}}$	$\dot{S}_{gen.Pu2} = \dot{m}_{17}(s_{19} - s_{18})$ $Exd_{Pu2} = \dot{W}_{Pu2} + Ex_{18} - Ex_{19}$

The entering fluids to the collector and from it to HST supposed to be equal the lowest and highest level's temperature of HST fluid, respectively.

$$T_{s.in} = T_{st1} \;\&\; T_{coll.in} = T_{st3} \tag{8}$$

$$\frac{\rho V_{HST}}{3} C_{p.Therminol-VP1} \frac{dT_{st1}}{dt} = \begin{bmatrix}\dot{m}_{coll} C_{p.Therminol-VP1}(T_{coll.out} - T_{st1}) + \dot{m}_s C_{p.Therminol-VP1}(T_{st2} - T_{st1})\\ -U_{HST} A_{HST}(T_{st1} - T_{Am})\end{bmatrix} \tag{5}$$

$$\frac{\rho V_{HST}}{3} C_{p.Therminol-VP1} \frac{dT_{st2}}{dt} = \begin{bmatrix}\dot{m}_{coll} C_{p.Therminol-VP1}(T_{st1} - T_{st2}) + \dot{m}_s C_{p.Therminol-VP1}(T_{st3} - T_{st2})\\ -U_{HST} A_{HST}(T_{st2} - T_{Am})\end{bmatrix} \tag{6}$$

$$\frac{\rho V_{HST}}{3} C_{p.Therminol-VP1} \frac{dT_{st3}}{dt} = \begin{bmatrix}\dot{m}_{coll} C_{p.Therminol-VP1}(T_{st2} - T_{st3}) + \dot{m}_s C_{p.Therminol-VP1}(T_{s.out} - T_{st3})\\ -U_{HST} A_{HST}(T_{st3} - T_{Am})\end{bmatrix} \tag{7}$$

Table 3
Capital cost of different system's components [67,72–74].

Equipment	Capital Cost	Reference Year	CEPCI of Ref. year
Ev	$\dot{Z}_{Ev} = \left(\frac{CEPCI_{2019}}{CEPCI_{2000}}\right)\left(Z_{ref.Ev}\left(\frac{A_i}{A_{ref}}\right)^{0.6}\right)$	2000	394.1
	$Z_{ref.Ev} = 16000$		
Co	$\dot{Z}_{Co} = \left(\frac{CEPCI_{2019}}{CEPCI_{2000}}\right)\left(Z_{ref.Co}\left(\frac{A_i}{A_{ref}}\right)^{0.6}\right)$	2000	394.1
	$Z_{ref.Co} = 8000$		
Ge	$\dot{Z}_{Ge} = \left(\frac{CEPCI_{2019}}{CEPCI_{2000}}\right)\left(Z_{ref.Ge}\left(\frac{A_i}{A_{ref}}\right)^{0.6}\right)$	2000	394.1
	$Z_{ref.Ge} = 17500$		
Ej	$\dot{Z}_{Ej} = \left(\frac{CEPCI_{2019}}{CEPCI_{2001}}\right)\left[\begin{matrix}1000 \times 16.14 \times 0.989\dot{m}_{Ge} \\ \times\left(\frac{T_{primary.flow}}{0.1P_{primary.flow}}\right)^{0.05}(0.1P_{exit})^{-0.75}\end{matrix}\right]$	2001	394.3
Pu	$\dot{Z}_{Pu} = \left(\frac{CEPCI_{2019}}{CEPCI_{2000}}\right)\left[2100\left(\frac{\dot{W}_{Pu}}{10}\right)^{0.26}\left(\frac{1-\eta_{Pu}}{\eta_{Pu}}\right)^{0.5}\right]$	2000	394.1
Ex.Va	$\dot{Z}_{Ex.Va} = \left(\frac{CEPCI_{2019}}{CEPCI_{2000}}\right)[114.5\dot{m}_{Ex.Va}]$	2000	394.1
ETC	$\dot{Z}_{ETC} = \left(\frac{CEPCI_{2019}}{CEPCI_{2012}}\right)[256.9A_{ETC}]$	2012	584.6
FPC	$\dot{Z}_{FPC} = \left(\frac{CEPCI_{2019}}{CEPCI_{2014}}\right)[235A_{FPC}]$	2014	576.1
PTC	$\dot{Z}_{PTC} = \left(\frac{CEPCI_{2019}}{CEPCI_{2009}}\right)[231.3A_{PTC}]$	2009	521.9
HST	$\dot{Z}_{HST} = \left(\frac{CEPCI_{2019}}{CEPCI_{2015}}\right)[578V_{HST}]$	2015	556.8
CST	$\dot{Z}_{CST} = \left(\frac{CEPCI_{2019}}{CEPCI_{2013}}\right)[60.69 * 10^{(2.9211\times\exp(0.1416\times\log V_{CST}))}]$	2013	567.3
AHU	$\dot{Z}_{AHU} = \left(\frac{CEPCI_{2019}}{CEPCI_{2007}}\right)[24202 \times A_{AHU}^{0.4162}]$	2007	525.4

Table 4
The various pollutant emission from electricity and their penalty cost [76].

	CO_2	NO_x	CO
ξ [kg /kWh]	0.7	0.3	0.004
C [$ /kg]	0.024	0.0208	6.853

The received heat by the generator is equal to:

$$Q_{Ge} = \dot{m}_s C_{p.Therminol-VP1}(T_{s.in} - T_{s.out}) \quad (9)$$

Also, it can be expressed as follows:

$$Q_{Ge} = (UA)_{Ge}\left(\frac{T_{s.in} - T_{s.out}}{\ln\left(\frac{T_{s.in}-T_{Ge}}{T_{s.out}-T_{Ge}}\right)}\right) \quad (10)$$

Where $(UA)_{Ge} = 1.5$ [kW /K].

- Cold storage tank

The closed-type CST was chosen with two charge and discharge processes [68–70] and two feed circuits to transfer and consume refrigerant. The stored cold in CST is equal to Ref. [64]:

$$Q_{CST} = \frac{\dot{Q}_{CD} \times \delta t_{CD}}{\eta_{CST}} \quad (11)$$

Where $\dot{Q}_{CD}$, δt_{dc} and η_{CST} are required refrigeration, discharge time and CST's efficiency, respectively. The CST capacity can be evaluated by:

$$V_{CST} = \frac{3600 \times \dot{Q}_{CST}}{(\rho_l C_l(T_{dc} - T_{s.l})) + \rho_l h_{s.l} + (\rho_s C_s(T_{s.l} - T_{CST}))} \quad (12)$$

Where $h_{s.l}$ represents fusion enthalpy.

Heat loss between CST fluid and surrounding is obtained by:

$$\dot{Q}_{le,ch/dc} = A_{CST}\frac{T_{Am} - T_{ch/dc}}{R_{th}} \quad (13)$$

The produced refrigerant is transferred to CST by the first feeding circuit during the charge process.

$$\Delta\dot{E}_{CST.ch} = \dot{Q}_{14-15} \quad (14)$$

In the discharge process, CD should be supplied by CST. Moreover, heat leakage between CST fluid and the environment is added to the discharge load.

$$\Delta\dot{E}_{CST.dc} = \dot{Q}_{17-19} + \dot{Q}_{le.ch} \quad (15)$$

Therefore, the net transferred heat from CST is equal to:

$$\dot{Q}_{CST} = \dot{Q}_{17-19} + \dot{Q}_{le.dc} - \dot{Q}_{14-15} \quad (16)$$

Three heat terms can transfer from CST's boundaries. Based on them, CST's entropy generation will calculate by:

$$\dot{S}_{gen.CST} = -\frac{1}{T_0}\dot{Q}_{le} - \frac{1}{T_{17}}\dot{Q}_{17-19} - \frac{1}{T_{15}}\dot{Q}_{14-15} \quad (17)$$

$$\dot{E}x_{d.CST} = T_0\dot{S}_{gen.CST} \quad (18)$$

3.1.4. General balance equations of various components

A summary of the energy and exergy balances for the ejector cycle's different components can be found in Table 2.

3.2. Economic, environmental, and exergo-economic analyses

A comprehensive economic analysis is carried out from two viewpoints (detailed and exergo-economic analyses). Followed by the environmental analysis is performed to achieve the system's usefulness from

Table 5
Exergo-economic with required auxiliary equations of the SEJHCST's components.

Equipment	Cost balance	auxiliary equations
Ev	$\dot{C}_6 + \dot{C}_{16} + \dot{Z}_{Ev} = \dot{C}_2 + \dot{C}_{14}$	$c_2 = c_6$ $c_{16} = 0.07042$
Co	$\dot{C}_3 + \dot{C}_7 + \dot{Z}_{Co} = \dot{C}_4 + \dot{C}_8$	$c_7 = c_8$
Ge	$\dot{C}_{12} + \dot{C}_5 + \dot{Z}_{Ge} = \dot{C}_1 + \dot{C}_{13}$	$c_{12} = c_{13}$
Ej	$\dot{C}_2 + \dot{C}_1 + \dot{Z}_{Ej} = \dot{C}_3$	–
Ej's Pu	$\dot{C}_4 + \dot{Z}_{Pu_{Ej}} + c_{W.Pu_{Ej}}\dot{W}_{Pu_{Ej}} = \dot{C}_5$	$c_{W.Pu_{Ej}} = c_{elec}$ $c_{elec} = 0.115$ \$/kWh [83]
Ex.Va	$\dot{C}_4 + \dot{Z}_{Ex.Va} = \dot{C}_6$	–
Coll	$\dot{C}_{\dot{Q}_{sol}} + \dot{C}_9 + \dot{Z}_{coll} = \dot{C}_{10}$	–
HST	$\dot{C}_{11} + \dot{C}_{13} + \dot{Z}_{HST} + \dot{C}_{\dot{Q}_{loss.HST}} = \dot{C}_9 + \dot{C}_{12}$	$c_9 = c_{11}$
Pu of coll circuit Coll circuit's Pu	$\dot{C}_{10} + \dot{Z}_{Pu_{coll}} + c_{W.Pu_{coll}}\dot{W}_{Pu_{coll}} = \dot{C}_{11}$	$c_{W.Pu.Coll} = c_{elec}$
Pu1	$\dot{C}_{15} + \dot{Z}_{Pu1} + c_{W.Pu1}\dot{W}_{Pu1} = \dot{C}_{16}$	$c_{W.Pu1} = c_{elec}$
Pu2	$\dot{C}_{18} + \dot{Z}_{Pu2} + c_{W.Pu2}\dot{W}_{Pu2} = \dot{C}_{19}$	$c_{W.Pu2} = c_{elec}$
CST	$\dot{C}_{14} + \dot{C}_{19} + \dot{Z}_{CST} = \dot{C}_{15} + \dot{C}_{17} - \dot{C}_{\dot{Q}_{le},CST} + \dot{C}_{fusion}$	$c_{17} = c_{19}$
AHU	$\dot{C}_{17} + \dot{C}_{20} + \dot{Z}_{AHU} = \dot{C}_{18} + \dot{C}_{21}$	$c_{20} = 0$

pollutant saving viewpoint.

In general, the system's economic-environmental balance is expressed by Ref. [69]:

$$\dot{C}_{total} = \sum_k \dot{Z}_{inv,k} + \dot{C}_{main} + \dot{C}_{op} + \dot{C}_{envr} \quad (19)$$

In the above equation, $\sum_k \dot{Z}_{inv,k}$, $\dot{C}_{op}$, $\dot{C}_{main}$ and $\dot{C}_{envr}$ represent the purchase costs of all equipment, operational, maintenance, and finally the environmental pollutant costs.

3.2.1. Detailed economic approach

A detailed economic approach includes several factors such as capital investment, installation and piping, operation and maintenance costs, capital recovery coefficient, salvage value, annual book depreciation, and the payback period [71]. Table 3 displays the capital costs of various components. These costs should be updated with the Chemical Engineering Plant Cost Index (CEPCI), which is 607.5 for 2019.

The capital recovery factor is expressed by below equation [75]:

$$CRF_{Capital} = \frac{i(1+i)^n}{(1+i)^n - 1} \quad (20)$$

Where lifetime and annual interest rate are shown by $n = 20$ and $i = 0.1$ [76]. An advanced method has been used to calculate the maintenance cost with a direct effect on annual interest factor, inflation rate, system lifetime and salvage value as follows [77,78]:

$$CRF_{O.M} = \left[\frac{1+r}{i-r}\right]\left[1 - \left(\frac{1+r}{1+i}\right)^n\right] \quad (21)$$

Where inflation rate is assumed to be equal to $r = 0.04$. Levelized total system capital cost is calculated from:

$$\dot{Z}_{total.2019.Capital} = \frac{CRF_{Capital}}{NN} Z_{total.2019} \quad (22)$$

Where $NN = 5544$ [h] and $Z_{total.2019}$ express annual system operation hours and capital cost. The piping and jointing's costs are assumed to be 10% of the purchasing equipment [79]. The levelized maintenance cost is calculated by:

$$\dot{Z}_{total.2019.O.M} = \frac{CRF_{O.M} \times f}{NN} \dot{Z}_{total.2019.Capital} \quad (23)$$

Where $f = 0.01$ is the maintenance factor related to purchase cost. The total cost can be reached as follows:

$$\dot{Z}_{total.2019.final} = \dot{Z}_{total.2019.Capital} + \dot{Z}_{total.2019.O.M} \quad (24)$$

3.2.2. Environmental approach

The significance of environmental analysis lies in how a system behaves toward the environmental problems, such as global warming and pollutants level [74,80]. In conventional EJC, the driven heat may provide by an auxiliary heater fed from grid electricity. Since electricity is generally produced by consuming fossil fuels, three pollutant kinds are considered namely CO_2, NO_x and CO. Therefore, the emission reduction should be estimated based on the pollutant emission factor (ξ) and the environmental tax factor (C) from electricity, recorded in Table 4.

An electric heater could consume electricity to provide desired heat as follows [81]:

$$\dot{W} = 8.42\dot{Q}^{0.87} \quad (25)$$

The electricity consumption by pumps should be subtracted from it. Therefore, the total annual penalty cost from the equivalent consumed

Table 6
DPR evaluation process and its formulation [71].

Variable	Equation
Salvage value	$SV = sv_0\left[\frac{\dot{Z}_{total.2019.Capital}}{CRF_{Capital}/NN}\right]$ $sv_0 = 0.1$ [78]
Total Capital Expenditure cost	$TCE_{total.SEJHCST} = \left[\frac{\dot{Z}_{total.2019.Capital}}{CRF_{Capital}/NN}\right] \times 1.1$
Total Depreciable Expenditure	$TDE = TCE_{total.SEJHCST} - SV$
Present Worth Factor	$PWF = \frac{1}{(1+i)^n}$
Annual Capital Cost	$ACC = PW \times CRF_{Capital}$
Annual Book Depreciation	$ABD = \frac{TDE}{n}$
Annual Net Cash Flow	$ANCF = CPW \times \dot{Q}_{sol.yearly}$
Average Annual Profit	$AAP = ANCF - ABD$
Average Rate of Return	$ARR = \frac{AAP}{\dot{C}_{total.SEJHCST} \times NN}$
Detailed Payback period Ratio	$DPR = \frac{TDE}{ANCF}$

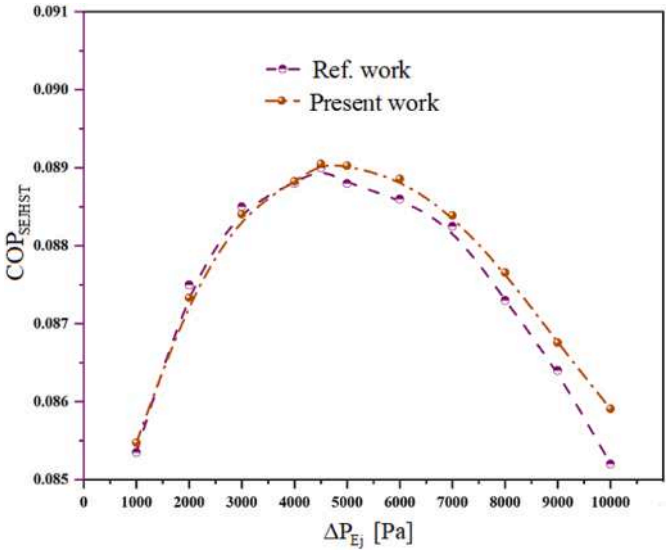

Fig. 3. Validation the results of the SEJHST system with Ref. [58].

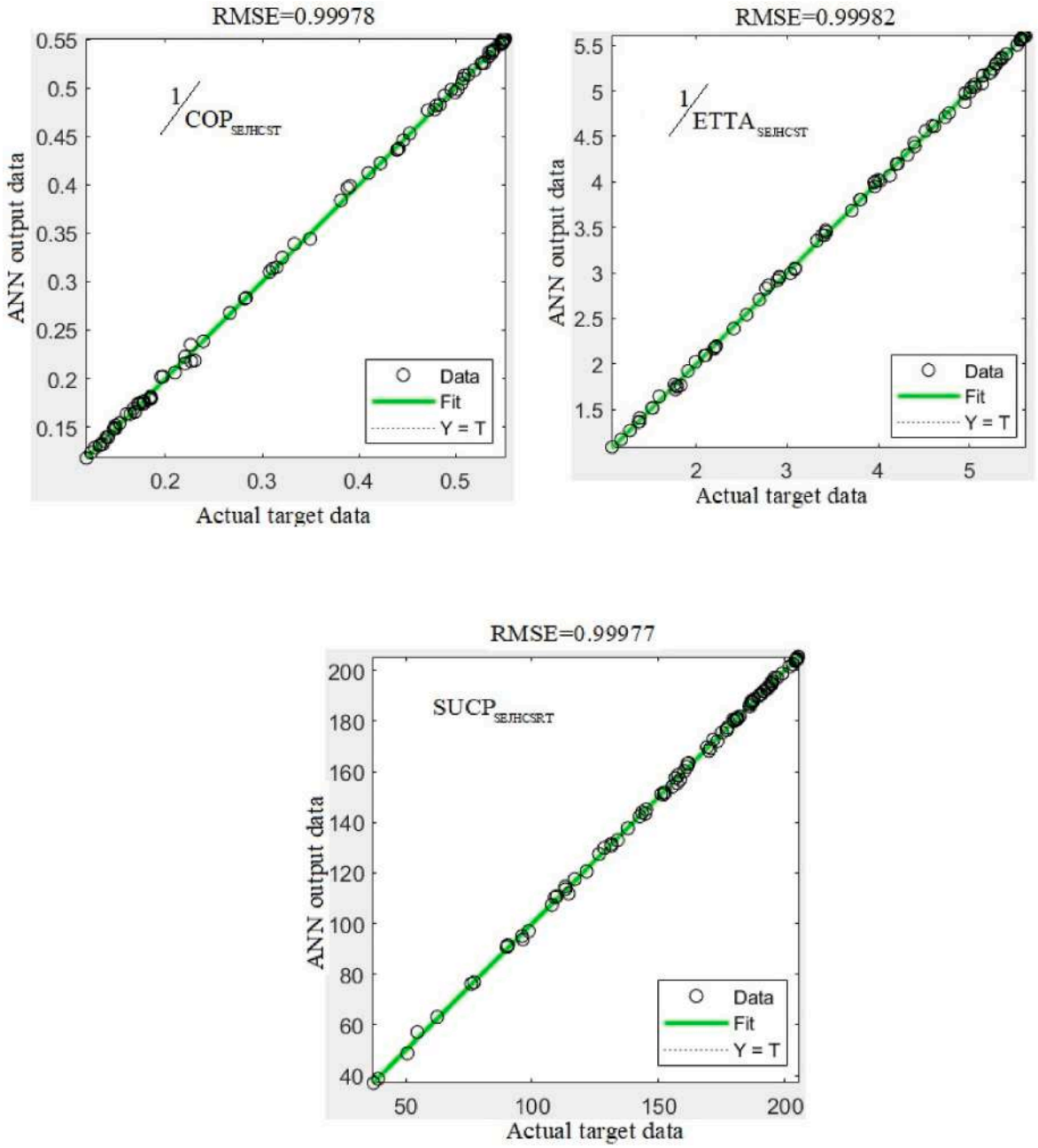

Fig. 4. Validation results between actual target and ANN output data for three objective functions by using PTC.

electricity is equal to Ref. [82]:

$$C_{envr} = \left[\left(\xi_{CO_2} \times C_{CO_2}\right) + \left(\xi_{CO} \times C_{CO}\right) + \left(\xi_{NO_x} \times C_{NO_x}\right)\right] \times \dot{W}_{total} \quad (26)$$

To levelize C_{envr} from dollar to dollar per year, we have:

$$\dot{C}_{envr} = C_{envr} \frac{CRF_{Capital}}{NN} \quad (27)$$

The system's total cost is determined by subtracting the saved penalty cost from total system cost as follows:

$$\dot{C}_{total.SEJHCST} = \dot{Z}_{total.2019.final} - \dot{C}_{envr} \quad (28)$$

3.2.3. Exergo-economic approach

In the exergo-economic approach, the average cost per unit of exergy (c [$/Wh]) for every outlet and inlet flow is multiplied to their exergy amount to evaluate the cost of exergy ($\dot{C}$ [$/h]). The general formulation of exergo-economic balance for all system components is expressed as follows [82]:

$$\sum \dot{C}_e + \dot{C}_w = \dot{C}_Q + \sum \dot{C}_i + \dot{Z} \quad (29)$$

The exergo-economic balance equations with their auxiliary relations have been listed in Table 5 for all system equipment.

3.2.4. Detailed payback period ratio

The recovery time to return system's cost is determined by payback period definition [71]. The formulation process of the Detailed Payback period Ratio (DPR) is represented in Table 6.

3.3. System performance assessment

Evaluating system performance requires appropriate criteria defining based on effective parameters. Due to show CST's role besides

Table 7
Initial assumptions for the SEJHCST modeling.

Collector, hot storage tank, and their feed circuits	
Sun temperature (T_{sun})	5780 K
Collector surface (A_{coll})	1000 m^2
Pump of collector circuit's efficiency ($\eta_{Pu_{coll}}$)	0.75
HST's volume (V_{HST})	40 m^3
Total heat transfer coefficient of generator ($(UA)_{Ge}$) [58]	1.5 kW/K
Thermal loss coefficient of HST (U_{th}) [58]	0.5 W/m^2.K
Ejector cycle	
Pressure drop (ΔP_{Ej})	4500 Pa
Suction and motive nuzzle's efficiencies (η_{mn} , η_{sn}) [86]	0.9
Mixing and diffuser sections efficiencies (η_m, η_d) [58]	0.85
Efficiency of EJC's pump ($\eta_{Pu_{Ej}}$)	0.85
T_{Ge}	70 ⟨T_{Ge}⟨130 °C
T_{Co}	35 ⟨T_{Co}⟨45 °C
T_{Ev}	− 5°C
T_7, P_7	T_{Am}, P_{Am}
T_8	T_4 + 8°C
Cold storage tank and its feed circuits	
T_{CST}	0°C
Total thermal resistance (R_{th}) [87]	1.980 m^2K/W
CST's efficiency (η_{CST})	0.95
Charge and discharge times (t_{ch}, t_{dc})	13 h, 15 h
Pump's efficiencies (η_{Pu1}, η_{Pu2})	0.85
Generator and evaporator's effectiveness (Eff_{Ev}, Eff_{Ge})	0.425
T_{16}	T_2 + 4°C
T_{17}	7°C
T_{18}	T_{11} + 5°C

PTC and zeotropic fluid in EJC performance, assessment criteria are reported for both EJC and SEJHCST. In the same vein, refrigeration production is the main goal of EJC, while CST's role and received heat by it would be examined in SEJHCST. For the integrated system, $\dot{Q}_{sol}$ is considered to evaluate $COP_{SEJHCST}$ contribute to all system components efficiency (e.g., collector, HST, CST and EJC). Please note that the criteria are evaluated as instaniously and daily forms.

According to the energy, exergy and economic-environmental aspects, below equations are defined for evaluating EJC and SEJHCST system:

$$COP_{Ej} = \frac{\dot{Q}_{Ev}}{\dot{Q}_{Ge}} \tag{30}$$

$$\eta_{ex.Ej} = \frac{Ex_{\dot{Q}_{Ev}}}{Ex_{\dot{Q}_{Ge}}} \tag{31}$$

$$COP_{SEJHCST} = \frac{\dot{Q}_{CST}}{\dot{Q}_{sol}} \tag{32}$$

$$\eta_{ex.SEJHCST} = \frac{Ex_{\dot{Q}_{CST}}}{Ex_{\dot{Q}_{sol}}} \tag{33}$$

$$SUCP_{SEJHCST} = \frac{Co_{CST} + Co_{air.Co} + Co_{env}}{Ex_{\dot{Q}_{CST}} + Ex_{\dot{Q}_{air.Co}}} \tag{34}$$

The cost of products, including unit cost per exergy multiply to the exergy amount of each stream, is defined by SUCP [84]. This criterion involves together exergo-economic and environmental. An air-cooled condenser is used to remove extra heat from EJC. The air temperature is changed significantly, which is able to use for desired goals. Also, the net saving of penalty cost can be added to the products category.

4. Validation

4.1. Thermodynamic validation

The SEJHST performance was validated by the results of Ref. [58]. Based on the solution procedure shown in Fig. 2, the appropriate entrainment ratio of the present study was calculated at various ejector pressure drops. Finally, COP_{SEJHST} was evaluated to compare two studies results based on Eq. (35).

$$COP_{SEJHST} = \frac{\dot{Q}_{Ev}}{\dot{Q}_{sol}} \tag{35}$$

As it can be seen in Fig. 3, the validation results of COP_{SEJHST} have good agreement with those reported by Ref. [58]. The maximum error was 2.36% which can be proved the high accuracy of the current study.

4.2. ANN approach validation

ANN approach is employed to train thermo-economic-environmental data and fit a reliable relation for triple-MPSO algorithm. The root mean square is a standard criterion for assessing the accuracy of ANN performance:

$$RMSE = \sqrt{\frac{\sum_{j=1}^{N} (y_{t,j} - y_{f,j})^2}{N}} \tag{36}$$

According to Fig. 4, the RMSE values are around 0.99977–0.99982, which represents high accuracy in validation results between actual target and ANN outputs.

5. Results and discussions

The thermo-economic and environmental analyses are an attempt to

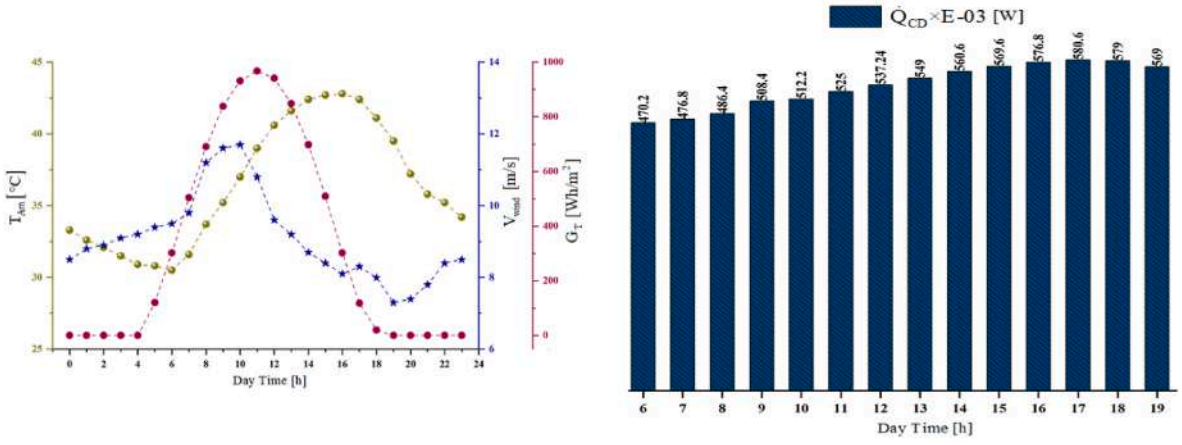

Fig. 5. Weather conditions and required CD of case study [88].

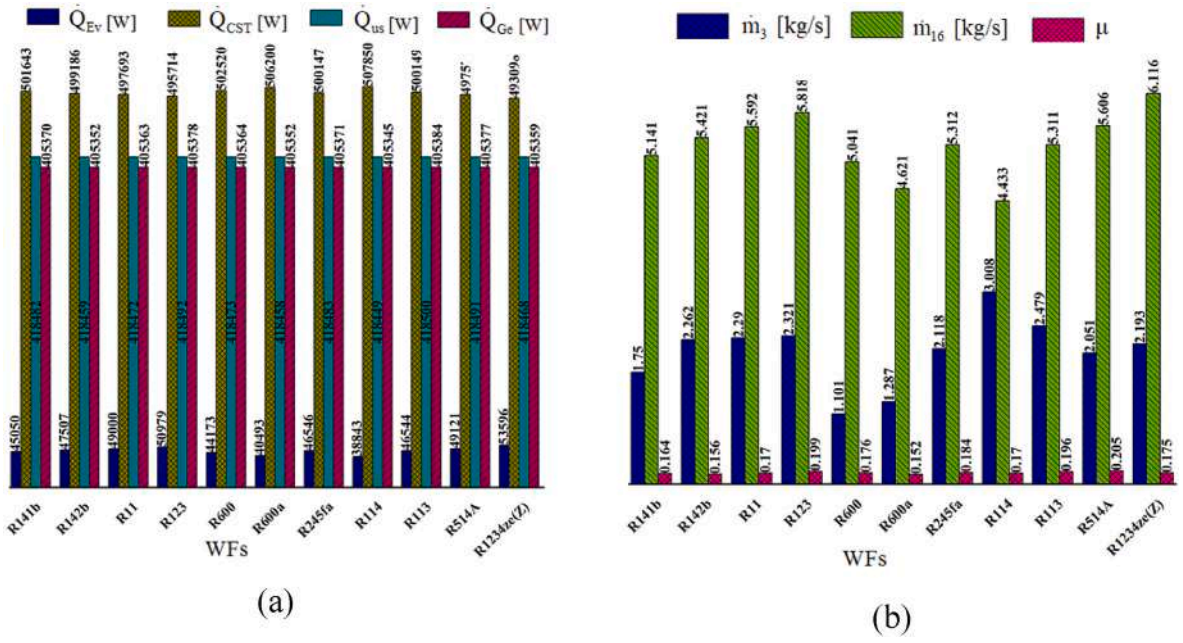

Fig. 6. Various WFs effects on system's loads and mass flow rates.

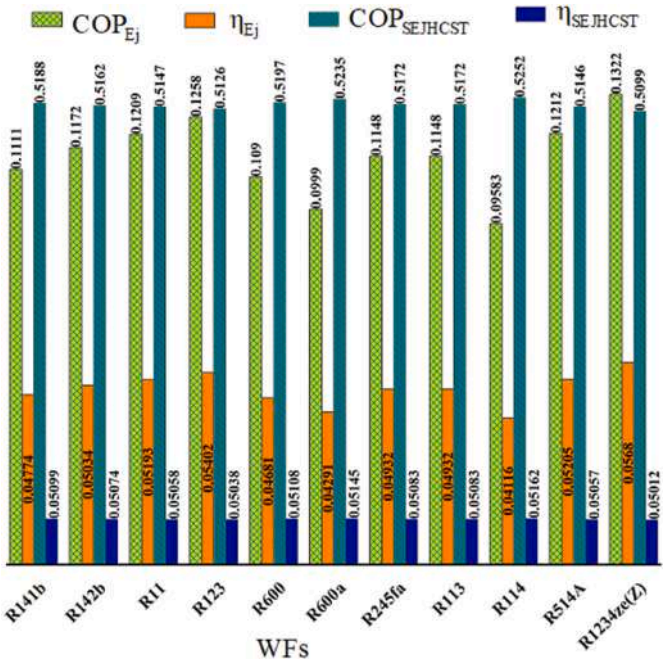

Fig. 7. Various WFs effects on system performance based on exergo-economic-environmental criteria.

represent the usefulness and superiority of each system [85]. Moreover, sensitivity analysis and multi-objective optimization can be helpful for evaluating system performance and determining the optimal conditions. The initial input parameters of SEJHCST are shown in Table 7.

5.1. Weather conditions and cooling demand

Zabol-Sistan in Iran has 300 sunny days in a year [88]. So, the Zabol region is classified in the high solar potential category made reasonable using SEJS. Due to variable solar intensity, the SEJHCST performance is analyzed under dynamic evaluation during a summer design day.

Fig. 5 presents CD for 5000 m^2 floor area of an educational building with comfortable indoor temperature below 23°C. The sunny hours begin from 5 a.m. to 6 p.m. The solar intensity is strong enough to attract by collector and produce heat during sunny hours. The cold can be produced at these sunny hours, which should be transferred to CST. Also, CD should be provided by CST under discharge hours from 6 a.m. to 8 p.m. The building requests maximum CD at 5 p.m. at which the outside dry-bulb temperature is high, and the solar intensity is declining. Remained heat in air molecules and building material's thermal storage capacity is the reason of the long time to heat transfer into indoor space.

5.2. Working fluid selection

Pure refrigerants were commonly used in EJC in previous studies [2, 89]. Using zeotropic fluids offer a feasible way to improve EJC's performance with decreasing phase change irreversibility [55] due to temperature glide [90]. The high boiling temperature and supercritical properties are advantages of the zeotropic fluid. Moreover, they have environmentally friendly properties. Bai et al. [91] and Liu et al. [56] studied the effects of various zeotropic mixture impacts on EJC's operation conditions and performance.

In the current study, more comprehensive kinds of WFs are investigated to select the best one for operation in SEJHCST. The various WFs ability in the production or transmission of heat is shown in Fig. 6(a). At the constant value of $\dot{Q}_{us}$, EJC has attracted maximum heat by R113 followed by R123 and R514A. The received heat to the generator acts as a system stimulator, which causes to produce refrigeration by the evaporator. The maximum cold is produced by R1234ze(Z), the following ranks belong to R123 and R514A. $\dot{Q}_{CST}$, being equal to CD and heat amount attracted by CST, has a reverse trend of $\dot{Q}_{Ev}$. All in all, R514A has the third rank of received and produced heat/cold of EJC by 8% maximum difference. Various WFs role in cold transmission completely coordinates with produced refrigeration, as shown in Fig. 6 (b). The higher value of μ causes the better performance of ejector. Its maximum amount belongs to R514A, followed by R123 and R113. Whereas the ejector xits mass flow rate ($\dot{m}_3$) is related to both suction and motive flows. So, its most considerable value occurs for R114.

For assessing of WFs operation, all energy, exergy, and economic criteria of EJC and SEJHCST are reported. As shown in previous figures,

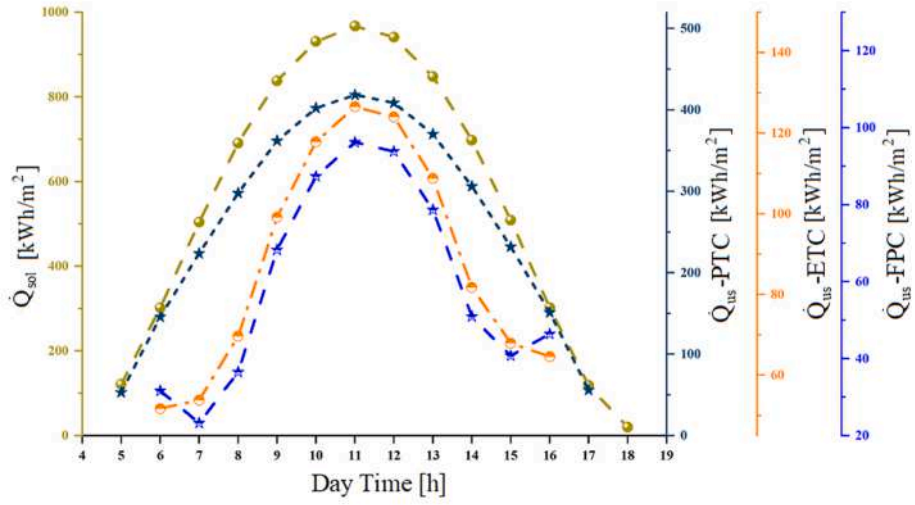

Fig. 8. The received useful heat from the sun radiation by various collectors.

Table 8
Various collector's effect on HST's and collector's operation characteristics.

	η_{coll} [%]	$T_{coll.out} = T_{10}$ [°C]	$T_{s.out} = T_{13}$ [°C]	T_{st1} [°C]	T_{st2} [°C]	T_{st3} [°C]
PTC	44.11	400.15	220.93	352.91	307.738	263.61
ETC	12.82	242.46	142.22	215.07	189.64	165.2
FPC	8.9	218.5	129.77	193.38	170.77	149.36

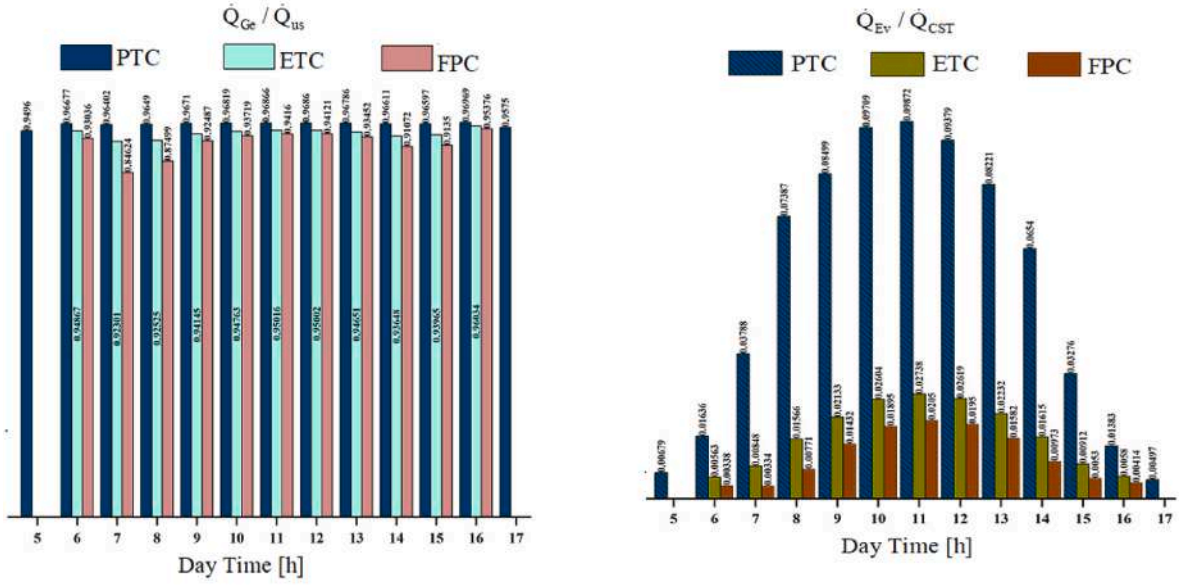

Fig. 9. The comparison of various collector's operation between received and produced heat/cold ratio for the SEJHCST.

WFs have direct effects on EJC as well as on SEJHCST characteristics. The maximum COP_{Ej} and η_{Ej} belong to R1234ze(Z), and the following ranks belong to R123 and R514A by 8% difference, while the second rank of the largest $COP_{SEJHCST}$ and $\eta_{SEJHCST}$ found for R514A by 2% difference with R114. Although R1234ze(Z) is an environmentally friendly WFs, SEJHCST represents better performance by using R514A. In comparison, ODP and GWP of R514A are not much different from those of R1234ze(Z). Since reducing the harmful environmental effects is primary goal of the present study, and also EJC and SEJHCST's COP and η_{ex} amounts for R514A are slightly different from the leaders, it was chosen as the best WF. Moreover, R514A belongs to the zeotropic fluid group, which is verified with high effectiveness in energy and exergy efficiencies [90], as improved in Fig. 7.

5.3. Sensitivity analysis

In this sub-section, design variables effects on system performance are investigated based on exergo-economic-environmental criteria and some main related parameters. The sensitivity analysis is a practical step in evaluating system performance and size improvement.

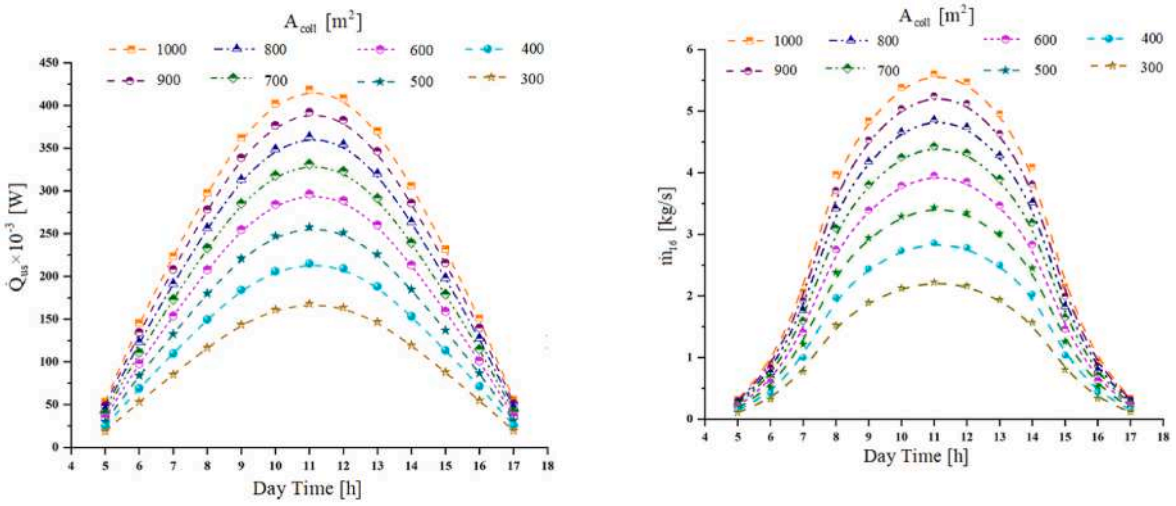

Fig. 10. The collector surface's effect on the dynamic behavior of received useful energy and mass flow rates of CST's circuit.

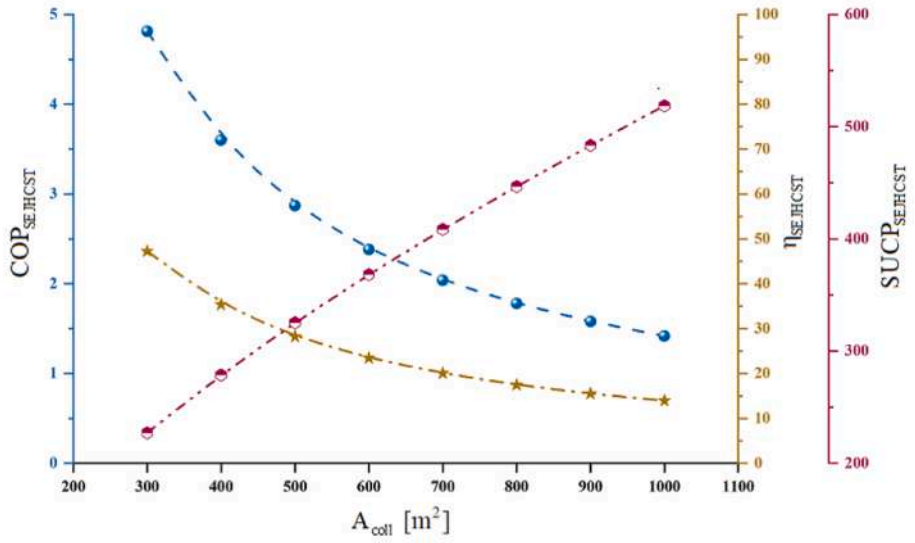

Fig. 11. Various collector surface on system performance based on exergo-economic-environmental criteria.

5.3.1. Various kinds of the collector

The three types of solar collector's impacts are evaluated on SEJHCST performance. Because the heat losses of FPCs are less than ETC types, the high temperature can be achieved by them. Concentrating solar technology has received less attention than FPCs and ETCs [2]. The sun tracking devices are used in this type of solar collector technology. Actually, high radiation levels can be reached in long intervals compared to non-concentrating collectors with fixed inclination by using PTCs [92].

Each collector kind can attain the global solar irradiance portion based on its technology characteristic and efficiency named useful energy. As can be seen in Fig. 8, the changing procedure of $\dot{Q}_{us}$ is the same as that of $\dot{Q}_{sol}$. PTC can attract more useful energy compared to other kinds. In addition, PTC can receive solar radiation in low values around 120 $[Wh/m^2]$ but FPC and ETC types have no performance at these conditions.

According to Eq. (2), the collector efficiency has direct and reverse relationships with working temperature and solar radiation, respectively. Due to concentrating effect, PTCs can reach to more temperatures in the same solar intensity compared to the other kinds. So that its efficiency should be higher than FPCs and ETCs. The higher efficiency causes the larger temperature at the collector outlet as well as for HST. Total daily efficiency of each collector kind, average daily temperature in HST and feed circuit of the generator are found in Table 8.

The FPC and ETC's efficiencies are about 20% and 30% those of PTC's. Similarly, the daily average produced exit temperature from PTC is significantly larger than that of two other kinds. Followed by the high distributed temperature is observed in HST. Finally, feed stream can nourish the generator with high temperatures at which the heat engine (generator) can work more efficiently [92]. This is proven by the generator received heat ratio to the useful solar energy, shown in Fig. 9. The generator highest value to the useful solar loads belongs to PTC, with the highest feed temperature followed by ETC and FPC.

Therefore, the temperature and pressure levels of the ejector primary flow are augmented. Also, entrainment ratio is enhanced, which would increase EJC efficiency. This means that the more refrigeration can be produced, the high evaporator load ratio is achievable to consume it from CST. The evaporator to stored loads ratio is significantly higher than that of two FPC and ETC kinds. According to PTC advantages in highly feed temperature accessibility, efficiency, and cold production, it is selected as the best choice due to having the best performance for

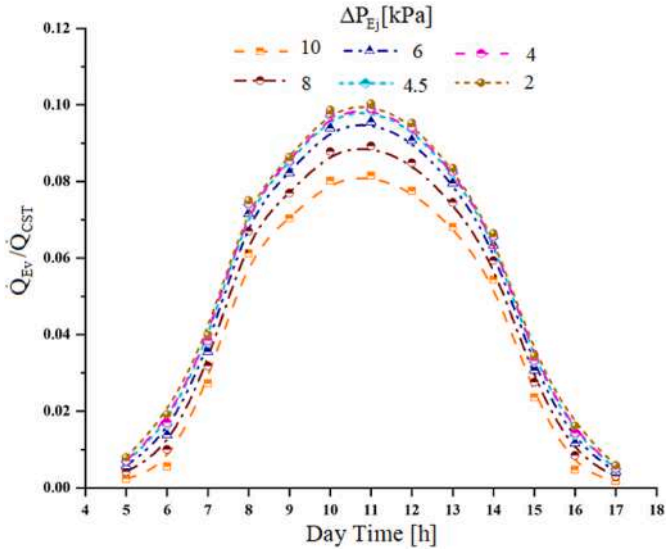

Fig. 12. Ejector pressure drop's impact on system dynamic behavior in produced/consumed refrigeration ratio.

SEJHCST. The purchase cost of PTC is about 0.8–8% more than two other kinds of collectors. Since FPC and ETC types may need an auxiliary heater [15], which imposes an extra cost on the system, the price difference between PTC and the two others can be ignored.

5.3.2. Different collector's surfaces

The received useful energy from the sun is dependent to the collector surface. As shown in Fig. 10, $\dot{Q}_{us}$ had been directly enhanced with increasing of the collector surface. The ejector primary mass flow rate is changed according to $\dot{Q}_{us}$ which causes an enhancement in refrigeration production. The more cold-production causes an increase in the mass flow rate of the first feed circuit between the evaporator and CST.

The collector surface's impacts on the energy, exergy and exergo-economic-environmental criteria are represented in Fig. 11. With increasing collector area, daily average values of $COP_{SEJHCST}$ and $\eta_{SEJHCST}$ decrease because of the reduction in $\dot{Q}_{store}$. The amount of $\dot{Q}_{Ev}$ decreases according to cold direction with a negative sign while the daily average of $\dot{Q}_{le}$ and $\dot{Q}_{CD}$ values have remained constant. Increasing of $SUCP_{SEJHCST}$ is not far from expected because it is directly proportional to component's expenditure cost.

5.3.3. Different ejector pressure drops

Due to various solar irradiations at sunny hours, the fed energy to EJC is changeable. To ensure optimal performance of EJC, the area ratio must be adjusted by changing in the entrainment ratio under varying operating conditions. Using a variable-geometry ejector is a viable solution to achieve it [93]. By referring to the ejector formulation represented in Fig. 2, this can be proven that the pressure drop has been related to the area ratio changing by its impact on the entrainment ratio, entropy and outlet secondary flow pressure. Therefore, pressure ratio changing can have effects on the ejector geometry. The amount of pressure drop (ΔP_{Ej}) is dependent on the ejector design, which determines the pressure ratio between the primary and secondary flows [58].

The produced/consumed refrigeration ratio decreases with increasing of ΔP_{Ej} whereas its changing procedure is similar to $\dot{Q}_{us}$ during interval time. The evaporator load amount enhances with reducing ΔP_{Ej} because the more substantial pressure ratio is achievable. More fluid can be sucked by suction nuzzle, entrainment ratio enhances, and the ejector device has better performance. Therefore, $\dot{Q}_{Ev}$ has enhanced with a negative sign, which rationalizes observed changes in Fig. 12. On the other hand, μ treats similar to $\dot{Q}_{Ev}$ as well as mass flow rates out of the ejector and also the feed circuit from the evaporator to CST (Fig. 13).

As the results of Fig. 14, EJC's COP and exergy efficiency have relationship with $\dot{Q}_{Ev}$ directly. Therefore, their changing procedures are similar to each other. Since the changing of $\dot{Q}_{CST}$ is adverse to $\dot{Q}_{Ev}$, the amounts of $COP_{SEJHCST}$ and $\eta_{SEJHCST}$ augment with pressure drop enhancement. $SUCP_{SEJHCST}$ amount changes with the inverse trend. The reduction of $\dot{Q}_{CST}$ causes a decreasing trend for it.

5.3.4. Various evaporator temperatures

One of the essential design parameters of SEHCST is evaporator temperature. Fig. 15 shows its effect on $\dot{Q}_{Ev}/\dot{Q}_{CST}$ ratio. Refrigeration load produces based on solar irradiation during sunny hours. Moreover, $\dot{Q}_{Ev}/\dot{Q}_{CST}$ shows a reducing procedure with the decrease of evaporator's temperature. The evaporator load decreases because of the lower fusion enthalpy in the more negative temperature of R514A. Following the reduction of $\dot{Q}_{Ev}$ with negative sign, $\dot{Q}_{CST}$ value should be increased. So, decreasing trend of $\dot{Q}_{Ev}/\dot{Q}_{CST}$ seems logical. The average daily mass flow rates of primary flow and feed circuit from evaporator to CST and also

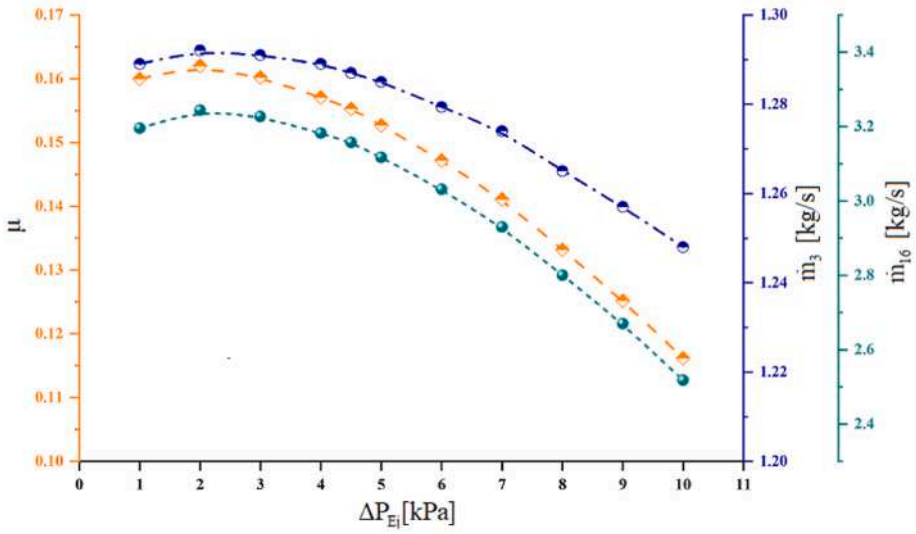

Fig. 13. The ejector pressure drop variation on μ, mass flow rates of the producer and carrier refrigeration.

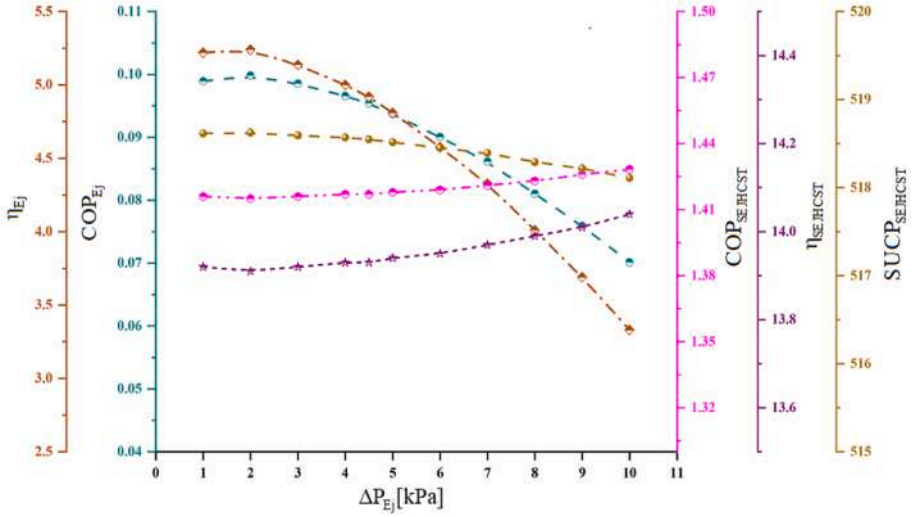

Fig. 14. Ejector pressure drop variation on system performance based on exergo-economic-environmental criteria.

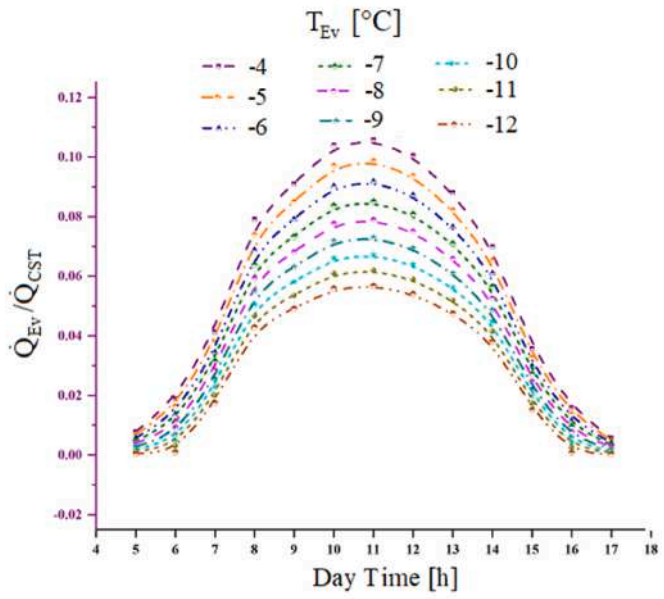

Fig. 15. Evaporator temperature variation on system dynamic behavior and produced/consumed refrigeration ratio.

entrainment ratio change with the same procedure as $\dot{Q}_{Ev}$, shown in Fig. 16.

Based on Fig. 17, COP and exergy efficiency of EJC change in accordance with T_{Ev} variations. Increasing evaporator temperature causes a reduction of them. Although $COP_{SEJHCST}$ and $\eta_{SEJHCST}$ descend, $SUCP_{SEJHCST}$ has ascended. Increasing of $\dot{Q}_{CST}$ can analyze the total system COP and exergy efficiency enhancement. It is also true for $SUCP_{SEJHCST}$, because its value relates to exergy of $\dot{Q}_{CST}$ directly which enhanced too.

5.3.5. Changing of HST capacity

HST capacity has no significant effect on system performance. As shown in Fig. 18, HST volume variation between 60− 25 m^3 causes the maximum increase in $\dot{Q}_{Ev}/\dot{Q}_{CST}$ ratio around 2%. The received solar radiation and the stored heat in HST fluid remains constant. At this condition, the larger HST volume means the lower inside fluid temperature. Stratified fluid's temperature behaves based on this fact (Fig. 19). Followed by lower heat can transfer to generator compared with upper HST fluid's temperature. When the motive power ($\dot{Q}_{Ge}$) to EJC reduces, less refrigeration ($\dot{Q}_{Ev}$) produces too. Same as before, the $\dot{Q}_{CST}$ value is increased by decreasing of $\dot{Q}_{Ev}$. To achieve an acceptable temperature, HST size should have the proper capacity. Because inadequate HST capacities can cause high temperatures and vice versa, the system operation can be made unfeasible. The HST sizing don't significantly improve the refrigeration production of the system, which it proved by Ref. [15] too (see Fig. 20).

With increasing HST volume, the change in reducing of $\dot{Q}_{Ge}$ and $\dot{Q}_{Ev}$ values happens similarly, which can be kept constant the amounts of COP_{SEJHST} and η_{SEJHST}. But with the increase of $\dot{Q}_{CST}$, the amounts of $COP_{SEJHCST}$, $\eta_{SEJHCST}$ and $SUCP_{SEJHCST}$ enhance.

5.4. Optimum design variables by using GA technique

A one-objective optimization is carried out to determine the best values of design parameters including T_{Ev}, V_{HST} and A_{coll}. The objective function is defined by considering all thermo-economic-environmental aspects as follows:

$$Inv_{EOF} = {}^{1}/_{[(w_1 \times \eta_{Ex.SEJHCST}) + (w_2 \times COP_{SEJHCST}) + (w_3 \times PSUC_{SEJHCST})]} \quad (37)$$

The weight coefficients show thermo-economic-environmental criteria's portion in Inv_{EOF} which they have equivalent share ($w_1 = w_2 = w_3 = 1/3$). Estimating of design conditions is performed for two values of ΔP_{Ej} including 2 kPa and 4.5 kPa. Moreover, the generator effectiveness impact is evaluated at each defined state in the optimum design values determination.

According to the results of Fig. 14, COP_{Ej} and η_{Ej} have their maximum values in 2 kPa whereas their changing's slop starts from 4.5 kPa amount sharply. Although, $COP_{SEJHCST}$ and $\eta_{SEJHCST}$ have almost their minimum values in 2 kPa, changing trend of them is very smooth and be at its middle state in 4.5 kPa. Table 9 represents the GA optimization results. The maximum difference value of Inv_{EOF} is about 1.5%. Also, few differences are observed for others design parameter at different optimized conditions. Since the more effectiveness of generator shows the better results and also has significant positive effect on system performance, the choice of final states is made between two evaluated states with big generator effectiveness. System design condition is based on the constant temperature in CST's fluid at 0° C. Not only the

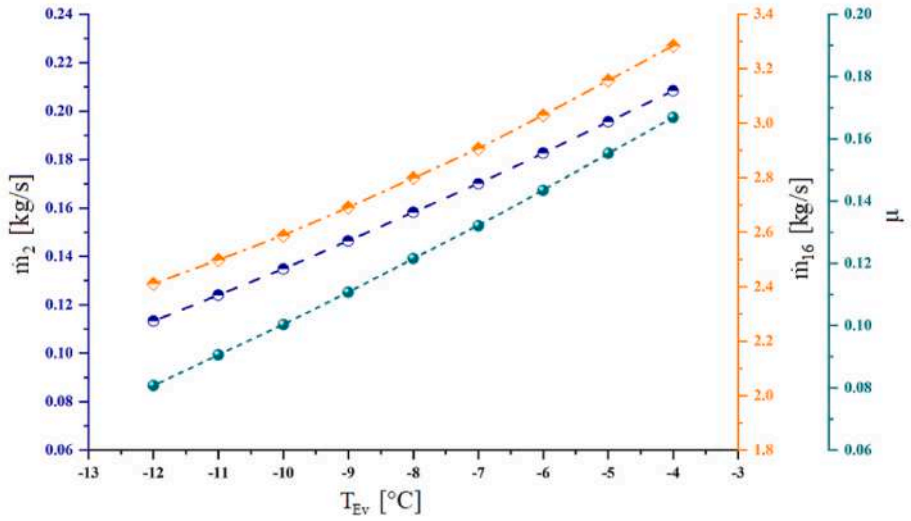

Fig. 16. Evaporator temperature effect on μ , mass flow rates of the producer and carrier refrigeration.

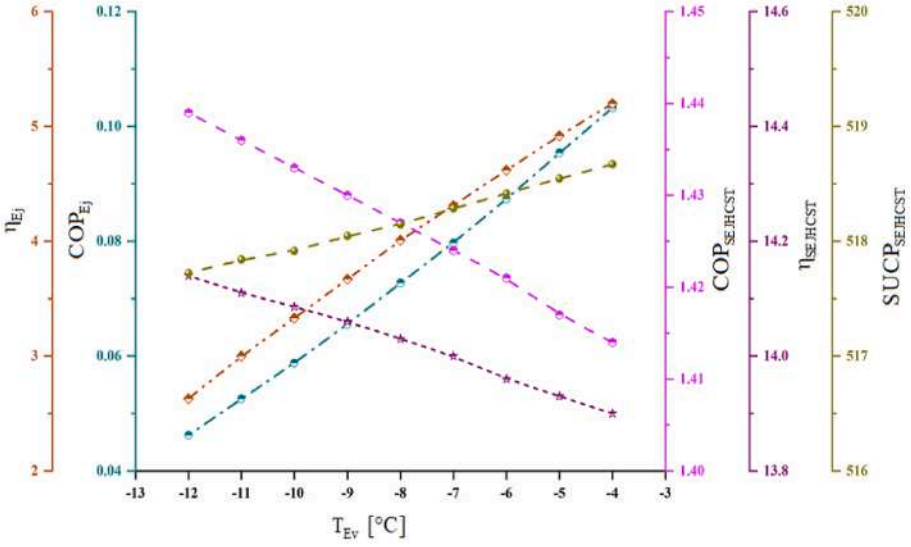

Fig. 17. Various evaporator temperature effects on system performance based on exergo-economic-environmental criteria.

evaporator's low-temperature does not be helpful for supplying CD, but also imposes a high cost on the system. Moreover, a low evaporator temperature can be obtained at low ejector pressure drop, which is desirable. Note the fact that the HST capacity is more considerable than the second state, it is ignored because of its small effect on total system cost and performance. Therefore, the best operation condition is chosen at maximum solar radiation time with $Eff_{Ge} = 0.425$ and $\Delta P_{Ej} =$ 2000 Pa. The COP, exergy, and sum unit cost per exergy of SEJHCST are equal to 1.81,17.17% and 205.3, respectively. It is proved that using of CST can enable reducing solar collector area [20].

5.5. Thermo-economic evaluation of the base SEJHCST

As the results shown in Table 10, using the collector and HST reduces the COP and exergy efficiency of SEJHST system compared to EJC due to collector losses. However, adding CST to SEJC with a HST increases the COP and exergy efficiency up to nine and two times their basic value, respectively. Therefore, despite the fact that 25% of the whole system cost is related to CST, it is logical to use both hot and cold storage tanks from a thermodynamic point of view. After estimating the best values of the operation parameters and substituting them in system modeling, the thermo-economic parameters are reported in Table 10 for various

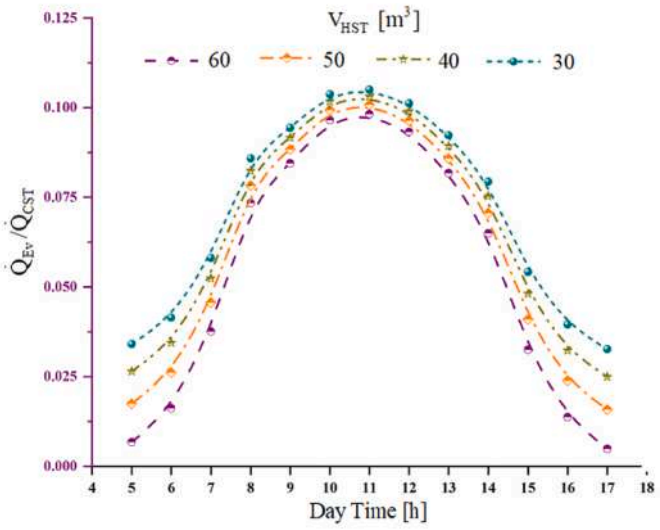

Fig. 18. HST capacity effects on system dynamic behavior and produced/consumed refrigeration ratio.

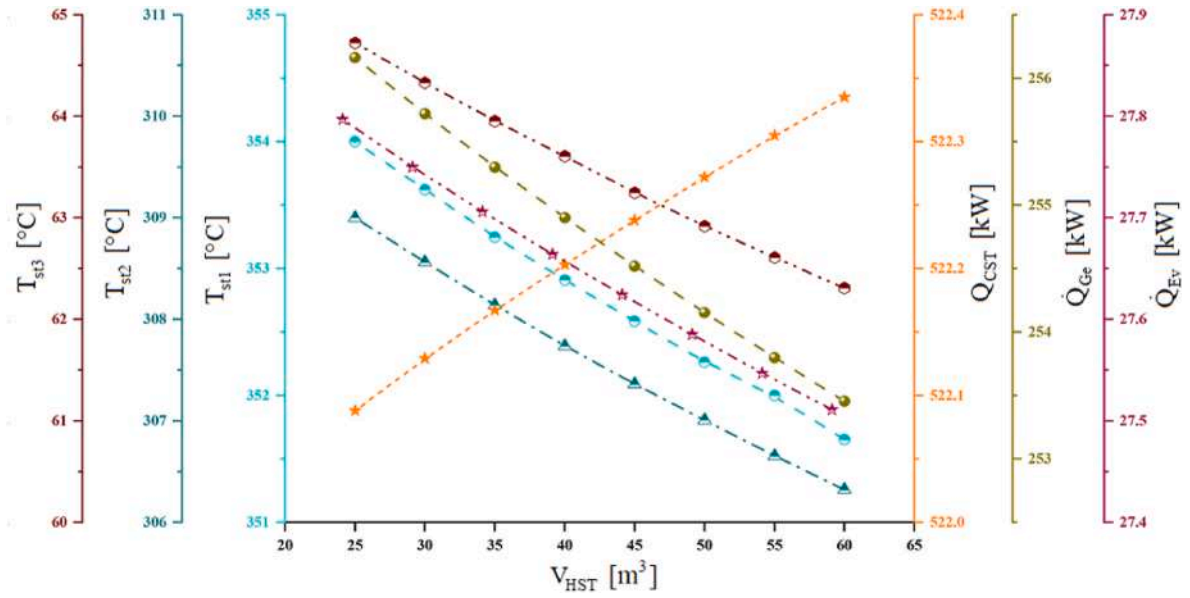

Fig. 19. HST volume effect on the operation loads and the system temperatures.

stream points. As can be seen in Table 11, the maximum and minimum unit costs per exergy belong to situations 8 and 4, respectively. Since, all removed heat from SEJHCST should have occurred from the condenser, the minimum and maximum unit costs per exergy are occurred between two sides of it. By feeding heat and raising the temperature, unit cost per exergy is enhanced and vice versa.

The portion of the various components' exergy destruction are presented in Fig. 21. The maximum of exergy destruction amount belongs to PTC and the next ones are the generator, AHU and CST. Actually, more than 80% of system exergy have been wasted by them.

Also, this system can save the penalty cost of environmental pollutants equal to 1.308E+07 [$/year] by taking into account to the grid electricity consumption of pumps and their pollutant costs. DPR of SEJHCST is evaluated about 3.5 years.

5.6. MPSO technique and the SEJHCST sizing

Employing multi-objective optimization is effective in setting goals to system future improvement because the effects of energy, exergy, and

Table 9
Optimum design parameters by using one-objective GA.

Variables	Best values from GA optimization results			
11 a.m. (Max. Solar radiation) $T_{Am} = 39°C - V_{Wind} = 10.8$ m/s, CD = 525 kW, $T_{Ge} = 130°C - T_{Co} = 45°C$, $G_T = 967$ Wh/m²	$Eff_{Ge} = 0.425$		$Eff_{Ge} = 0.225$	
$1000 < \Delta P_{Ej} < 10000$	**2000**	**4500**	**2000**	**4500**
$-12 < T_{Ev} < -4$	−6	−10.11	−11.83	−10.58
$300 < A_{coll} < 1000$	301.7	300.2	300.4	301.4
$25 < V_{HST} < 60$	58.34	36.23	50.66	56.48
Collector types	PTC	PTC	PTC	PTC
Inv_{EOF}	1.505	1.482	1.482	1.488

Table 10
Daily COP and exergy efficiency of various sub-system.

	EJC	SEJHST	SEJHCST
COP	0.1085	0.04628	1.008
η_{ex} [%]	4.835	0.5767	9.908

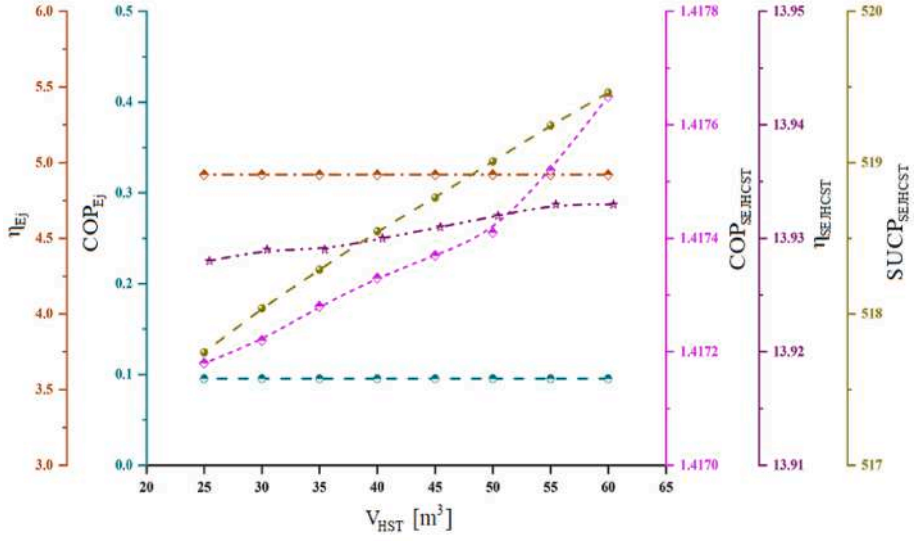

Fig. 20. HST capacity variation on system performance based on exergo-economic-environmental criteria.

Table 11
Thermo-economic characteristics at different state points of the SEJHCST.

stream	T [°C]	P [kPa]	h [kJ/kg]	s [kJ/kg.K]	Ex [kW]	C [$/year]	c [$/W.year]
1	130	1.46E+03	491.121	1.799	36.155	33123	0.9161
2	−6	23.267	391.702	1.719	−2.843	11.96	0.004209
3	88.31	175.314	474.759	1.867	13.862	33136	2.39
4	45	175.314	251.762	1.175	0.418	6.91E-09	1.65E-11
5	45.69	1.46E+03	252.960	1.176	1.04	524.6	0.5044
6	−6	23.267	251.762	1.195	−0.683	2.878	0.004209
7	39	101.325	312.657	5.742	−1.78E04	5.14E+04	2.896
8	53	101.325	326.738	5.786	−1.77E04	5.14 + 04	2.896
9	225.7	395.493	390.310	1.005	93.955	14119	0.1503
10	339.8	297.427	649.103	1.471	274.247	40873	0.149
11	340.8	405.300	652.75	1.475	276.613	41568	0.1503
12	299	405.300	553.777	1.310	207.671	41308	0.1989
13	191	395.493	319.808	0.858	44.694	8890	0.1989
14	−2	2.03E+03	−6.407	0.031	8.012	350.32	0.05279
15	0.9565	2.02E+03	6.035	0.0147	6.636	840.1	0.1049
16	0.9569	2.03E+03	6.046	0.015	6.636	467.3	0.07042
17	7	202.650	29.626	0.106	62.271	17320	0.2781
18	12	87.275	50.493	0.181	30.402	8937	0.294
19	12.6	202.650	51.262	0.183	32.561	9056	0.2781
20	39	101.325	39.211	5.742	11.938	0	0
21	25	101.325	25.117	5.694	15.692	15190	0.968

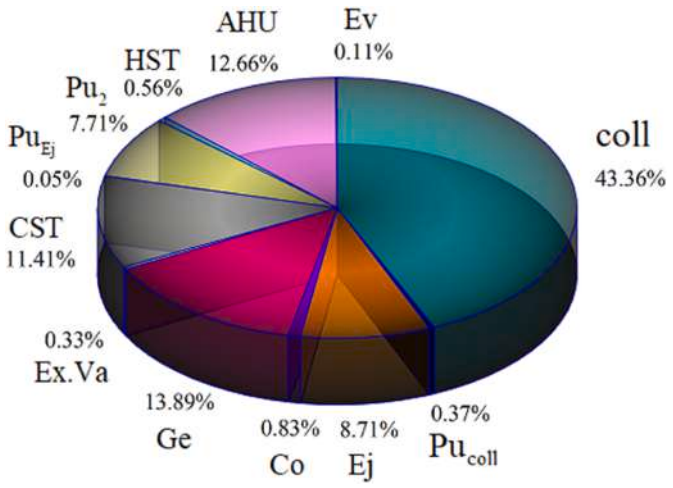

Fig. 21. Exergy destruction of SEJHCST's various components.

economic-environmental criteria are separately evaluated [94]. PSO technique has some advantages such as fast convergence, efficient in memory requirements, and speed [91]. SEJHCST performance is optimized by applying a triple-objective MPSO technique. Three objective functions, including the inverse of COP, exergy efficiency and also SUCP, should be minimized. These parameters conflict with each other.

Fig. 22 represents the optimization results of SEJHCST performance. SEJHCST can be divided into three sub-systems including collector and HST's circuit, EJC and CST and its circuit. System sizing means each of them should have optimum values. $\dot{Q}_{us}$ and $\dot{m}_{coll}$ are considered as the first sub-system's size symbols as well as $\dot{m}_2$ and V_{CST} for the other two ones. Please note that all design parameters optimum amounts had been determined during variable interval in GA optimization step except the effect of collector kinds. The collector kind's effect on system performance is appraised in present section. The best value of the objective functions and various parameters representing system sizing can be obtained in Table 12. PTC has a better data distribution in the optimization space and higher performance than two other kinds. $COP_{SEJHCST}$ and $\eta_{SEJHCST}$ values of PTC are around 2.3–3 times those of FPC and ETC, while its economic criterion (SUCP) is about 1.1 times bigger than that of PTC and around 0.6 times of ETC.

More collector mass flow rate can be flowed in less absorbed useful energy from the sun by using PTC. Not only ETC can absorb more useful energy but also it needs a high EJC's size. The size of EJC is lower for FPC and PTC compared to ETC which is an advantage. The size of V_{CST} has almost the same value for all types of collectors. All in all, the optimal performance and sizing values of SEJHCST belong to PTC type.

6. Conclusion

The dynamic behaviors of a solar-powered ejector cycle integrated with hot and cold storage tanks (SEJHCST) were investigated to supply building refrigeration in Zabol-Iran. Firstly, a comprehensive study on different WFs were carried out focused on CST's role in SEJHCST performance as well as various kinds of solar collector. Then, two-stage optimizations were performed to determine the optimum parameters, including design variables through a sensitivity analysis beside the one-objective GA. After substituting them in thermo-economic-environmental modeling, system sizing and also exergo-economic-environmental assessment criteria were estimated by the triple-objective MPSO algorithm.

Considering the results, the following points could be made:

- ✓ PTC selection as a heat source for EJC was based on its ability to operate effectively in a broad range of solar radiation, to achieve high feed temperatures, and to produce cold efficiently.
- ✓ R514A was identified as the best WF from the zeotropic category with the environmentally friendly properties. Due to having good temperature glide, zeotropic fluid can handle variations of solar intensity and phase changing processes.
- ✓ From sensitivity analysis results, the maximum and minimum effects on $COP_{SEJHCST}$, $SUCP_{SEJHCST}$ and $\eta_{SEJHCST}$ belonged to A_{coll} and V_{HST}, respectively. Although ΔP_{Ej} had the largest impact on COP_{EJ} and η_{Ej}, its effects on exergo-economic-environmental criteria of SEJHST had the next rank after T_{Ev}.
- ✓ Optimum design variables were determined with significant reduction of about 70% and 55% for A_{coll} and ΔP_{Ej} and 46% augmentation for V_{HST} compared to their initial guesses.
- ✓ Maximum exergy destruction belonged to PTC with 43.36% followed by AHU and CST.
- ✓ Although ETC could be able to attract more useful energy from the sun, the EJC's and CST had smaller sizes with using PTC compared to it. This despite the fact that SEJHCST had its maximum COP and exergy efficiency at various component's optimum size values with

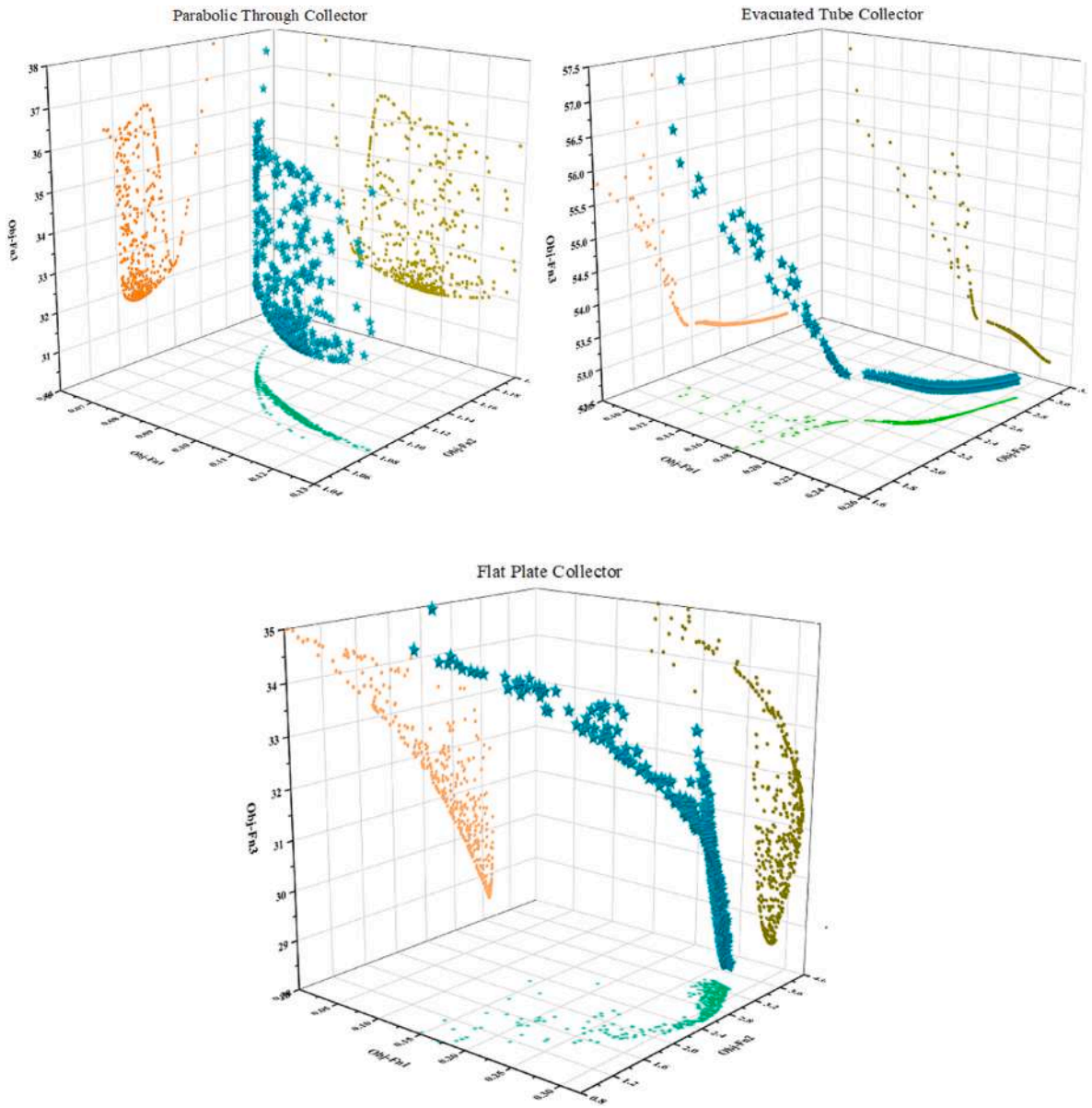

Fig. 22. Pareto frontier for various collectors by using triple-objective MPSO.

Table 12
Best optimized values for different sub-system's sizes and overall thermo-economic performance criteria.

	Best Objective-Function 1 $COP_{SEJHCST}$	Best Objective-Function 2 $\eta_{SEJHCST}$ [%]	Best Objective-Function 3 $SUCP_{SEJHCST}$ [$/h]	Sizing Parameter of Collector $\dot{Q}_{us}$ [kW]	Sizing Parameter of EJC $\dot{m}_2$ [kg/s]	Sizing Parameter of HST $\dot{m}_{coll}$ [kg/s]	Sizing Parameter of CST V_{CST} [m^3]
PTC	9.45	91.37	31.67	18.944	0.006	0.50	96.45
ETC	4.06	34.34	52.85	62.77	0.00958	0.40	98.28
FPC	3.53	30.37	28.46	14.56	0.0059	0.101	89.34

PTC case. Moreover, SUCP was about half that of ETC value. FPC had the lowest operation characteristic, which it disqualified.

✓ The cold tank's effectiveness was such that the SEJHCST's COP was enhanced up to three times compared to the ejector cycle at optimum design variable while exergy efficiency was reduced by half due to large exergy destruction of the collector.

✓ The system was able to significantly reduce the pollutant penalty cost by around 13 million dollars per year.

Credit author statement

Seyyedeh Mohadeseh Miri: Writing – original draft, Writing – review & editing, Visualization, Methodology, Validation, Software, Investigation, Mahmood Farzaneh-Gord: Supervision, Project administration, Formal analysis, Writing – review & editing, Visualization, Methodology, Ali Kianifar: Supervision

Declaration of competing interest

The authors declare that they have no known competing financial interests or personal relationships that could have appeared to influence the work reported in this paper.

Data availability

Data will be made available on request.

References

[1] Abdulateef JM, Sopian K, Alghoul MA, Sulaiman MY. Review on solar-driven ejector refrigeration technologies. Renew Sustain Energy Rev 2009;13:1338–49. https://doi.org/10.1016/j.rser.2008.08.012.

[2] Braimakis K. Solar ejector cooling system. Renew Energy 2020;20:31504. https://doi.org/10.1016/j.renene.2020.09.079. 4.

[3] Besagni G, Mereu R, Inzoli F. Ejector refrigeration: a comprehensive review. Renew Sustain Energy Rev 2016;53:373–407. https://doi.org/10.1016/j.rser.2015.08.059.

[4] Huang BJ, et al. System performance and economic analysis of solar-assisted cooling/heating system. Sol Energy 2011;85(11):2802–10. https://doi.org/10.1016/j.solener.2011.08.011.

[5] Van Nguyen V, Varga S, Soares J, Dvorak V, Oliveira AC. Applying a variable geometry ejector in a solar ejector refrigeration system. Int J Refrig 2020;113:187–95. https://doi.org/10.1016/j.ijrefrig.2020.01.018.

[6] Golchoobian H, Behbahaninia A, Amidpour M, Pourali O. Dynamic exergy analysis of a solar ejector refrigeration system with hot water storage" Progress in sustainable energy technologies: generating renewable energy. Springer International Publishing; 2014. p. 327–37.

[7] Alexis GK, Karayiannis EK. A solar ejector cooling system using refrigerant R134a in the Athens area. Renew Energy 2005;30:1457–69.

[8] Ersoy HK, Yalcin S, Yapici R, Ozgoren M. Performance of a solar ejector cooling-system in the southern region of Turkey. Appl Energy 2007;84:971–83.

[9] Pollerberg C, Heinzel A, Weidner E. Model of a solar driven steam jet ejector chiller and investigation of its dynamic operational behaviour. Sol Energy 2009;83:732–42.

[10] Guo J, Shen HG. Modeling solar-driven ejector refrigeration system offering air conditioning for office buildings. Energy Build 2009;41:175–81. 2009.

[11] Chen X, Omer S, Worall M, Riffat S. Recent developments in ejector refrigeration technologies. Renew Sustain Energy Rev 2013;19:629–51. https://doi.org/10.1016/j.rser.2012.11.028.

[12] Varga S, Oliveira AC, Diaconu B. Analysis of a solar-assisted ejector cooling system for air conditioning. Int J Low Carbon Technol 2009;4:2–8.

[13] Vidal H, Colle S, Pereira GDS. Modelling and hourly simulation of a solar ejector cooling system. Appl Therm Eng 2006;26:663–72.

[14] Dorantes R, Estrada CA, Pilatowsky I. Mathematical simulation of a solar ejector-compression refrigeration system. Appl Therm Eng 1996;16:669–75. 1996.

[15] Pridasawas W, Lundqvist P. A year-round dynamic simulation of a solar driven ejector refrigeration system with iso-butane as a refrigerant. Int J Refrig 2007;30:840–50.

[16] Bellos E, Tzivanidis C. Parametric analysis and optimization of a solar driven trigeneration system based on ORC and absorption heat pump. J Clean Prod 2017;17:31102. https://doi.org/10.1016/j.jclepro.2017.05.159. 2.

[17] Bellos E, Tzivanidis C, Antonopoulos KA. Exergetic, energetic and financial evaluation of a solar driven absorption cooling system with various collector types. Appl Therm Eng 2016;102:749–59. https://doi.org/10.1016/j.applthermaleng.2016.04.032.

[18] Allouche Y, Varga S, Bouden C, Oliveira AC. Dynamic simulation of an integrated solar-driven ejector based air conditioning system with PCM cold storage. Appl Energy 2017;190:600–11.

[19] Diaconu BM, Varga S, Oliveira AC. Numerical simulation of a solar-assisted ejector air conditioning system with cold storage. Energy 2011;36:1280–91.

[20] Dennis M, Garzoli K. Use of variable geometry ejector with cold store to achieve high solar fraction for solar cooling. Int J Refrig 2011;34:1626–32.

[21] Mark Worall IWE. "An experimental investigation of a jet-pump thermal (ice) storage system powered by low-grade heat. In: Proceedings of the 3rd international conference on sustainable energy technologies"; 2004. p. 28–30. Nottingham, UK.

[22] Eames IW, Worall M, Wu S. An experimental investigation into the integration of a jet-pump refrigeration cycle and a novel jet-spay thermal ice storage system. Appl Therm Eng 2012. https://doi.org/10.1016/j.applthermaleng.

[23] Chen X, Worall M, Omer S, Su Y, Riffat S. Experimental investigation on PCM cold storage integrated with ejector cooling system. Appl Therm Eng 2014;63:419–27.

[24] Huang BJ, Petrenko VA, Samofatov IY, Shchetinina NA. Collector selection for solar ejector cooling system. Sol Energy 2001;71:269–74.

[25] Pridasawas W, Lundqvist P. An exergy analysis of a solar-driven ejector refrigeration system. Sol Energy 2004;76:369–79.

[26] Tashtoush B, Alshare A, Al-Rifai S. Hourly dynamic simulation of solar ejector cooling system using TRNSYS for Jordanian climate. Energy Convers Manag 2015;100:228–99. 2015.

[27] Ma X, Zhang W, Omer SA, Riffat SB. Experimental investigation of a novel steam ejector refrigerator suitable for solar energy applications. Appl Therm Eng 2010;30:1320–5.

[28] YapIcI R, Ersoy HK, Aktoprakoglu A, HalkacI HS, Yigit O. Experimental determination of the optimum performance of ejector refrigeration system depending on ejector area ratio. Int J Refrig 2008;31:1183–9.

[29] Jia Y, Wenjian C. Area ratio effects to the performance of air-cooled ejector refrigeration cycle with R134a refrigerant. Energy Convers Manag 2012;53:240–6.

[30] Varga S, Oliveira AC, Diaconu B. Numerical assessment of steam ejector efficiencies using CFD. Int J Refrig 2009;32:1203–11.

[31] Cizungu K, Groll M, Ling ZG. Modelling and optimization of two-phase ejectors for cooling systems. Appl Therm Eng 2005;25:1979–94.

[32] Varga S, Oliveira AC, Ma X, Omer SA, Zhang W, Riffat SB. Experimental and numerical analysis of a variable area ratio steam ejector. Int J Refrig 2011;34:1668–75.

[33] Varga S, Oliveira AC, Diaconu B. Influence of geometrical factors on steam ejector performance – a numerical assessment. Int J Refrig 2009;32:1694–701.

[34] Pianthong K, Seehanam W, Behnia M, Sriveerakul T, Aphornratana S. Investigation and improvement of ejector refrigeration system using computational fluid dynamics technique. Energy Convers Manag 2007;48:2556–64.

[35] Rusly E, Aye L, Charters WWS, Ooi A. CFD analysis of ejector in a combined ejector cooling system. Int J Refrig 2005;28:1092–101.

[36] Eames IW, Ablwaifa AE, Petrenko V. Results of an experimental study of an advanced jet-pump refrigerator operating with R245fa. Appl Therm Eng 2007;27:2833–40.

[37] Bartosiewicz Y, Aidoun Z, Desevaux P, Mercadier Y. Numerical and experimental investigations on supersonic ejectors. Int J Heat Fluid Flow 2005;26:56–70.

[38] Riffat SB, Gan G, Smith S. Computational fluid dynamics applied to ejector heat pumps. Appl Therm Eng 1996;16:291–7.

[39] Riffat SB, Omer SA. CFD modelling and experimental investigation of an ejector refrigeration system using methanol as the working fluid. Int J Energy Res 2001;25:115–28.

[40] Sriveerakul T, Aphornratana S, Chunnanond K. Performance prediction of steam ejector using computational fluid dynamics: Part 1 Validation of the CFD results. Int J Therm Sci 2007;46:812–22.

[41] Riffat SB, Everitt P. Experimental and CFD modelling of an ejector system for vehicle air conditioning. J Inst Energy 1999;72:41–7.

[42] Zhu Y, Cai W, Wen C, Li Y. Numerical investigation of geometry parameters for design of high-performance ejectors. Appl Therm Eng 2009;29:898–905.

[43] Kasperski J. Two kinds of gravitational ejector refrigerator stimulation. Appl Therm Eng 2009;29:3380–5.

[44] Shen S, Qu X, Zhang B, Riffat S, Gillott M. Study of a gas-liquid ejector and its application to a solar-powered bi-ejector refrigeration system. Appl Therm Eng 2005;25:2891–902.

[45] Wang F, Shen S. A novel solar bi-ejector refrigeration system and the performance of the added injector with different structures and operation parameters. Sol Energy 2009;83:2186–94.

[46] Huang BJ, Hu SS, Lee SH. Development of an ejector cooling system with thermal pumping effect. Int J Refrig 2006;29:476–84.

[47] Wang JH, Wu JH, Hu SS, Huang BJ. Performance of ejector cooling system with thermal pumping effect using R141b and R365mfc. Appl Therm Eng 2009;29:1904–12.

[48] Yu J, Chen H, Ren Y, Li Y. A new ejector refrigeration system with an additional jet pump. Appl Therm Eng 2006;26:312–9.

[49] Yu J, Li Y. A theoretical study of a novel regenerative ejector refrigeration cycle. Int J Refrig 2007;30:464–70.

[50] Ziapour BM, Abbasy A. First and second laws analysis of the heat pipe/ejector refrigeration cycle. Energy 2010;35:3307–14.

[51] Sokolov M, Hershgal D. Enhanced ejector refrigeration cycles powered by low grade heat. Part 2 design procedures. Int J Refrig 1990;13:357–63.

[52] Kairouani L, Elakhdar M, Nehdi E, Bouaziz N. Use of ejectors in a multievaporator refrigeration system for performance enhancement. Int J Refrig 2009;32:1173–85.

[53] Liu Y, Xin T, Cao L, Wan C, Zhang M. Compression-injection hybrid refrigeration cycles in household refrigerators. Appl Therm Eng 2010;30:2442. 7.

[54] Liu Y, Yu J. Performance evaluation of an ejector subcooling refrigeration cycle with zeotropic mixture R290/R170 for low-temperature freezer applications. Appl Therm Eng 2019;161:114128. https://doi.org/10.1016/j.applthermaleng.2019.114128. 2019.

[55] Yu M, Yu J. Thermodynamic analyses of a flash separation ejector refrigeration cycle with zeotropic mixture for cooling applications. Energy Convers Manag 2021;229:113755. https://doi.org/10.1016/j.enconman.2020.113755.

[56] Liu B, Guo X, Xi X, Sun J, Zhang B, Yang Z. Thermodynamic analyses of ejector refrigeration cycle with zeotropic mixture. Energy 2023;263:125989. https://doi.org/10.1016/j.energy.2022.125989.

[57] Tashtoush BM, Al-Nimr MA, Khasawneh MA. A comprehensive review of ejector design, performance, and applications. Appl Energy 2019;240:138–72. https://doi.org/10.1016/j.apenergy.2019.01.185.

[58] Bellos E, Tzivanidis C. Optimum design of a solar ejector refrigeration system for various operating scenarios. Energy Convers Manag 2017;154:11–24. https://doi.org/10.1016/j.enconman.2017.10.057.

[59] Bejan A, Tsatsaronis G, Moran M. Thermal design and optimization. John Wiley & Songg, INC; 1996.

[60] Bi Y, Yu M, Wang H, Huang J, Lyu T. Experimental investigation of ice melting system with open and closed ice-storage tanks combined internal and external ice melting processes, vol. 194. Energy Build.; 2019. p. 12–20. https://doi.org/10.1016/j.enbuild.2019.04.009.

[61] MacPhee D, Dincer I. Performance assessment of some ice TES systems. Int J Therm Sci 2009;48(12):2288–99. https://doi.org/10.1016/j.ijthermalsci.2009.03.012. 2009.
[62] Tashtoush B, Alshare A, Al-Rifai S. Performance study of ejector cooling cycle at critical mode under superheated primary flow. Energy Convers Manag 2015;94: 300–10. https://doi.org/10.1016/j.enconman.2015.01.039.
[63] Saleh B. Performance analysis and working fluid selection for ejector refrigeration cycle. Appl Therm Eng 2016;107:114–24. https://doi.org/10.1016/j.applthermaleng.2016.06.147.
[64] Miri SM, Farzaneh-gord M, Kianifar A. Evaluating the dynamic behaviour of wind-powered compression refrigeration cycle integrated with an ice storage tank for air conditioning application. Energy Convers Manag 2022;269:116093. https://doi.org/10.1016/j.enconman.2022.116093.
[65] Galindo J, Dolz V, García-Cuevas LM, Ponce-Mora A. Numerical evaluation of a solar-assisted jet-ejector refrigeration system: screening of environmentally friendly refrigerants. Energy Convers Manag 2020;210:112681. https://doi.org/10.1016/j.enconman.2020.112681.
[66] Shirazi A, Taylor RA, White SD, Morrison GL. A systematic parametric study and feasibility assessment of solar-assisted single-effect, double-effect, and triple-effect absorption chillers for heating and cooling applications. Energy Convers Manag 2016;114:258–77. https://doi.org/10.1016/j.enconman.2016.01.070.
[67] Bellos E, Tzivanidis C, Moschos K, Antonopoulos KA. Energetic and financial evaluation of solar assisted heat pump space heating systems. Energy Convers Manag 2016;120:306–19. https://doi.org/10.1016/j.enconman.2016.05.004.
[68] Yan G, Bai T, Yu J. Energy and exergy efficiency analysis of solar driven ejectorcompressor heat pump cycle. Sol Energy 2016;125:243–55. https://doi.org/10.1016/j.solener.2015.12.021.
[69] Sanaye S, Shirazi A. Thermo-economic optimization of an ice thermal energy storage system for air conditioning applications. Energy Build 2013;60:100–9. https://doi.org/10.1016/j.enbuild.2012.12.040.
[70] Wang X, Yu J. An experimental investigation on a novel ejector enhanced refrigeration cycle applied in the domestic refrigerator-freezer. Energy 2015;93: 202–9. https://doi.org/10.1016/j.energy.2015.09.038.
[71] Khalilzadeh S, Hossein Nezhad A. Utilization of waste heat of a high-capacity wind turbine in multi effect distillation desalination: energy, exergy and thermo-economic analysis. Desalination 2018;439:119. https://doi.org/10.1016/j.desal.2018.04.010. 37.
[72] Ebrahimi-Moghadam A, Moghadam AJ, Farzaneh-Gord M, Aliakbari K. Proposal and assessment of a novel combined heat and power system: energy, exergy, environmental and economic analysis. Energy Convers Manag 2020;204:112307. https://doi.org/10.1016/j.enconman.2019.112307.
[73] Aminyavari M, Najafi B, Shirazi A, Rinaldi F. Exergetic, economic and environmental (3E) analyses, and multi-objective optimization of a CO2/NH3 cascade refrigeration system. Appl Therm Eng 2014;65(1–2):42–50. https://doi.org/10.1016/j.applthermaleng.2013.12.075.
[74] Xu Y, Guo F, Song M, Jiang N, Wang Q, Chen G. Exergetic and economic analyses of a novel modified solar-heat-powered ejection-compression refrigeration cycle comparing with conventional cycle. Energy Convers Manag 2018;168:107–18. https://doi.org/10.1016/j.enconman.2018.04.098.
[75] Liu X, Yang X, Yu M, Zhang W, Wang Y, Cui P, et al. Energy, exergy, economic and environmental (4E) analysis of an integrated process combining CO2 capture and storage, an organic Rankine cycle and an absorption refrigeration cycle. Energy Convers Manag 2020;210:112738. https://doi.org/10.1016/j.enconman.2020.112738.
[76] Ghafurian MM, Niazmand H. New approach for estimating the cooling capacity of the absorption and compression chillers in a trigeneration system. Int J Refrig 2017;17:30480–2. https://doi.org/10.1016/j.ijrefrig.2017.11.026.
[77] Rostami S, Rostamzadeh H, Fatehi R. A new wind turbine driven trigeneration system applicable for humid and windy areas , working with various nano fl uids. J Clean Prod 2021;296:126579. https://doi.org/10.1016/j.jclepro.2021.126579.
[78] Mohamadi H, Saeedi A, Firoozi Z, Sepasi S, Veisi S. Heliyon Assessment of wind energy potential and economic evaluation of four wind turbine models for the east of Iran. Heliyon 2021;7:e07234. https://doi.org/10.1016/j.heliyon.2021.e07234.
[79] Jain V, Sachdeva G, Kachhwaha SS. Energy, exergy, economic and environmental (4E) analyses based comparative performance study and optimization of vapor compression-absorption integrated refrigeration system. Energy 2015;91:816–32. https://doi.org/10.1016/j.energy.2015.08.041.
[80] Sanaye S, Khakpaay N. Thermo-economic multi-objective optimization of an innovative cascaded organic Rankine cycle heat recovery and power generation system integrated with gas engine and ice thermal energy storage. J Energy Storage 2020;32:101697. https://doi.org/10.1016/j.est.2020.101697.
[81] Śmierciew K, Gagan J, Butrymowicz D, Karwacki J. Experimental investigations of solar driven ejector air-conditioning system. Energy Build 2014;80:260–7. https://doi.org/10.1016/j.enbuild.2014.05.033.
[82] Ebrahimi-moghadam A, Jabari A, Farzaneh-gord M. Comprehensive techno-economic and environmental sensitivity analysis and multi-objective optimization of a novel heat and power system for natural gas city gate stations. J Clean Prod 2020;262:121261. https://doi.org/10.1016/j.jclepro.2020.121261.
[83] Xu Y, Li Z, Chen H, Lv S. Assessment and optimization of solar absorption-subcooled compression hybrid cooling system for cold storage. Appl Therm Eng 2020;180:115886. https://doi.org/10.1016/j.applthermaleng.2020.115886.
[84] Ghaebi H, Parikhani T, Rostamzadeh H. A novel trigeneration system using geothermal heat source and lique fi ed natural gas cold energy recovery : energy , exergy and exergoeconomic analysis. Renew Energy 2018;119:513–27. https://doi.org/10.1016/j.renene.2017.11.082.
[85] Jiang Y, Ma Y, Han F, Ji Y, Cai W, Wang Z. Assessment and optimization of a novel waste heat stepped utilization system integrating partial heating sCO 2 cycle and ejector refrigeration cycle using zeotropic mixtures for gas turbine. Energy 2023; 265:126326. https://doi.org/10.1016/j.energy.2022.126326.
[86] Alexis GK. Estimation of ejector ' s main cross sections in steam-ejector refrigeration system. Appl Therm Eng 2004;24:2657–63. https://doi.org/10.1016/j.applthermaleng.2004.03.012.
[87] Kang Z, Wang R, Zhou X, Feng G. Research status of ice-storage air-conditioning system. Procedia Eng 2017;205:1741–7. https://doi.org/10.1016/j.proeng.2017.10.020.
[88] https://www.data.irimo.ir/.
[89] Yan G, Bai T, Yu J. Thermodynamic analysis on a modified ejector expansion refrigeration cycle with zeotropic mixture (R290/R600a) for freezers. Energy 2016;95:144–54. https://doi.org/10.1016/j.energy.2015.11.067.
[90] Huang Y, et al. Performance explorations of an organic Rankine cycle featured with separating and mixing composition of zeotropic mixture. Energy 2022;257: 124535. https://doi.org/10.1016/j.energy.2022.124535.
[91] Bai H, Luo S, Zhao X, Zhao G, Gao Y. Comprehensive assessment of a green cogeneration system based on compressed air energy storage (CAES) and zeotropic mixtures. Energy 2022;254:124190. https://doi.org/10.1016/j.energy.2022.124190.
[92] Infante C, Kim D. Techno-economic review of solar cooling technologies based on location-specific data 5 ′ conomique des technologies du froid Synthe ′ sur des donne ′ es spe ′ cifiques a ′ la localisation solaire base. Int J Refrig 2013:1–15. https://doi.org/10.1016/j.ijrefrig.2013.09.033.
[93] Chen J, Havtun H, Palm B. Investigation of ejectors in refrigeration system: optimum performance evaluation and ejector area ratios perspectives. Appl Therm Eng 2014;64(1–2):182–91. https://doi.org/10.1016/j.applthermaleng.2013.12.034.
[94] Mosaffa AH, Farshi LG. Exergoeconomic analysis and optimization of a novel integrated two power/cooling cogeneration system using zeotropic mixtures. Energy 2022;253:124132. https://doi.org/10.1016/j.energy.2022.124132.